ISSN 1854-6250

APEM journal

Advances in Production Engineering & Management

Volume 9 | Number 4 | December 2014

University of Maribor

Published by PEI
apem-journal.org

Advances in Production Engineering & Management

Identification Statement

APEM journal

ISSN 1854-6250 | Abbreviated key title: **Adv produc engineer manag** | Start year: 2006
ISSN 1855-6531 (on-line)

Published quarterly by **Production Engineering Institute (PEI)**, **University of Maribor**
Smetanova ulica 17, SI – 2000 Maribor, Slovenia, European Union (EU)

Phone: 00386 2 2207522, Fax: 00386 2 2207990
Language of text: English

University of Maribor

APEM homepage: apem-journal.org
University homepage: www.um.si

APEM Editorial

Subscription Rate: 120 EUR for 4 issues (worldwide postage included); 30 EUR for single copies (plus 10 EUR for postage); for details about payment please contact: info@apem-journal.org

Postmaster: Send address changes to info@apem-journal.org

Cover and interior design by Miran Brezocnik
Printed by Tiskarna Koštomaj, Celje, Slovenia

APEM journal is indexed/abstracted in **Inspec**, **EBSCO** (Academic Search Alumni Edition, Academic Search Complete, Academic Search Elite, Academic Search Premier, Engineering Source, Sales & Marketing Source, TOC Premier), **ProQuest** (CSA Engineering Research Database – Cambridge Scientific Abstracts, Materials Business File, Materials Research Database, Mechanical & Transportation Engineering Abstracts, ProQuest SciTech Collection), and **TEMA** (DOMA). Listed in **Ulrich's** Periodicals Directory and **Cabell's** Directory. The APEM journal was positively evaluated for inclusion in the **Scopus** (Elsevier) database.

University of Maribor
Production Engineering Institute (PEI)

Advances in Production Engineering & Management

Volume 9 | Number 4 | December 2014 | pp 155–204

Contents

Scope and topics **158**

Laser cladding of Ti-6Al-4V alloy with vanadium carbide particles **159**
El-Labban, H.F.; Mahmoud, E.R.I.; Al-Wadai, H.

Parametric study of die sinking EDM process on AISI H13 tool steel using statistical techniques **168**
Bose, G.K.; Mahapatra, K.K.

Effect of welding variables on mechanical properties of low carbon steel welded joint **181**
Talabi, S.I.; Owolabi, O.B.; Adebisi, J.A.; Yahaya, T.

A Petri net model for the integration of purchasing, production and packaging using Kanban system **187**
Ullah, H.

Calendar of events **201**

Notes for contributors **203**

Journal homepage: apem-journal.org

ISSN 1854-6250
ISSN 1855-6531 (on-line)

Scope and topics

Advances in Production Engineering & Management (*APEM journal*) is an interdisciplinary refereed international academic journal published quarterly by the *Production Engineering Institute* at the *University of Maribor*. The main goal of the *APEM journal* is to present original, high quality, theoretical and application-oriented research developments in all areas of production engineering and production management to a broad audience of academics and practitioners. In order to bridge the gap between theory and practice, applications based on advanced theory and case studies are particularly welcome. For theoretical papers, their originality and research contributions are the main factors in the evaluation process. General approaches, formalisms, algorithms or techniques should be illustrated with significant applications that demonstrate their applicability to real-world problems. Although the *APEM journal* main goal is to publish original research papers, review articles and professional papers are occasionally published.

Fields of interest include, but are not limited to:

Additive Manufacturing Processes
Advanced Production Technologies
Artificial Intelligence
Assembly Systems
Automation
Cutting and Forming Processes
Decision Support Systems
Discrete Systems and Methodology
e-Manufacturing
Fuzzy Systems
Human Factor Engineering, Ergonomics
Industrial Engineering
Industrial Processes
Industrial Robotics
Intelligent Systems
Inventory Management
Joining Processes
Knowledge Management
Logistics
Machine Tools
Machining Systems
Manufacturing Systems
Mechanical Engineering
Mechatronics
Metrology
Modelling and Simulation
Numerical Techniques
Operations Research
Operations Planning, Scheduling and Control
Optimisation Techniques
Project Management
Quality Management
Queuing Systems
Risk and Uncertainty
Self-Organizing Systems
Statistical Methods
Supply Chain Management
Virtual Reality

APEM journal
Advances in Production Engineering & Management
Volume 9 | Number 4 | December 2014 | pp 159–167
http://dx.doi.org/10.14743/apem2014.4.184
ISSN 1854-6250
Journal home: apem-journal.org
Original scientific paper

Laser cladding of Ti-6Al-4V alloy with vanadium carbide particles

El-Labban, H.F. [a], **Mahmoud, E.R.I.** [a,*], **Al-Wadai, H.** [a]

[a]Faculty of Engineering, King Khalid University, Abha, Saudi Arabia

ABSTRACT

The tribological properties of Ti-6Al-4V alloy are generally poor. This study was an attempt to produce a hardened surface layer on this alloy for longer service life during severe wear conditions. For this purpose, laser surface cladding of this alloy with vanadium carbide (VC) powder was performed using a YAG Fiber laser at power strengths of 1000 W, 1500 W, and 2000 W and a travelling speed of 4 mm/s. Surface cladded layers of Ti-6Al-4V alloy metal matrix composite reinforced with VC particles were produced on the substrate under all processing conditions. The size of the cladding layer was increased by increasing the processing power. The cladding layer was well bonded to the substrate, especially at higher processing powers. The VC particles were homogenously distributed within the cladding layer at processing powers of 2000 W and 1500 W, whilst it showed some clusters at a power of 1000 W. Some of the VC particles were melted and re-solidified as fine long dendritic structures during the laser treatment. The cladding layer produced under all processing conditions exhibits remarkable improvement of hardness and wear resistance (almost twice). As the processing powers decreased, the surface of the cladding layers showed higher hardness. The cladding layer also showed improved corrosion resistance.

ARTICLE INFO

Keywords:
Laser cladding
Ti-6Al-4V alloy
VC powder
Surface microhardness
Wear and corrosion resistance

**Corresponding author:*
emahoud@kku.edu.sa
(Mahmoud, E.R.I.)

Article history:
Received 2 August 2014
Revised 29 October 2014
Accepted 10 November 2014

1. Introduction

Titanium and its alloys are used for manufacturing of some components in automobile, aerospace, marine, medicine, chemical and energy industries, due to their improved properties such as high strength-to-weight ratio, excellent corrosion resistance, high temperature strength, high Young's modulus and high cycle fatigue properties [1-3]. Ti-6Al-4V alloy is considered the most used alloy in these applications. However, the uses of this alloy in the severe environments, where the wear is the main failure mode, are limited due to its poor wear resistance [4]. To overcome this problem, it is necessary to improve the surface wear resistance. Many different traditional surface modifications such as surface hardening [5] and surface cladding [6, 7] are applied to improve wear and erosion characteristics of the surfaces of Ti alloys. Various techniques such as thermal spraying [8], plasma spraying [9], traditional arc welding and focused energy technologies like electron beam [10] and laser [11-13] have been employed. The excessive energy input from the traditional welding processes such as shielded metal arc welding or even gas tungsten arc welding may cause some undesirable distortion and residual thermal stresses which may cause cracks in the hardened layer [6, 7]. Laser surfacing has been suggested as a potential technique to produce a hard surface layer of Ti alloys for a number of reasons. The most important one arises from the fact that laser beam has rapid heating and cooling, which

can easily produce special types of microstructure with novel properties that cannot be produced by other conventional processing technique [14, 15]. Generally, the obtained microstructure in the laser treated area is dependent on the heating and cooling cycles that take place during the process, which in consequence depends on the laser parameters [16]. Other merits of the laser surfacing are to produce a hard layer with low dilution and deformation, relative cleanliness, lack of quenching medium and limited grain growth during the heating [11].

Laser cladding process is considered one of the laser surfacing techniques that can produce Ti alloy-based composites clad layer where hard particles such as carbides, borides, and nitrides are used to reinforce the Ti alloy [17]. In this case, the wear properties can be improved by the combination of embedded hard carbide particles and the rapid heating and cooling which forms hard structure matrix. The widely used carbide particles as reinforcement are titanium carbide (TiC) and vanadium carbide (VC). VC possess many favorable properties, such as high hardness (2460-3150 $HV_{0.05}$) [18], high melting temperature (2830 °C) [19], low heat conductivity [20], certain plasticity, and good wettability to metal bonding. Moreover, VC has a low-friction coefficient [21]. Besides, when VC is used in high temperatures, it is oxidized to vanadium oxide (V_2O_5), which is characterized by self-lubrication performance [22, 23]. This advantageous combination can create a protective coating layer on the surface of the composite material with enhanced resistance against thermal, corrosion and mechanical wear [24, 25].

Thus, in the present study, we aim to investigate the effects of main laser parameters and rapid solidification on the microstructure, hardness and wear behaviour of Ti-6Al-4V alloy surface cladded by VC powder. Microstructural changes in the build-up, melted, and heat affected zones are examined in details.

2. Experimental work

Specimens of Ti-6Al-4V alloy were used as substrate with dimensions of 100 mm × 50 mm × 3 mm. The surfaces of specimens were cleaned and the oxides were removed by grinding using emery papers. In order to avoid the oxidation of the strip during the treatment, argon with the flowing rate of 15 L/min was used as a shielding gas during and after the treatment. The cladding treatment was carried out using VC powder with 40-50 μm particle size as a cladding material and YAG Fiber laser (Ytterbium laser system, YLS-3000 SM, 3 kW). The powder was preplaced on the top surface of the strip with 0.5 mm height and then emitted by laser beam. The treatments were conducted at different laser power strenghts of 1000 W, 1500 W, and 2000 W, and at fixed travelling speed of 4 mm/s. The process was conducted at a defocusing distance (D_f) of 24 mm. The microstructures of the coated layer and substrates were investigated using optical microscope and scanning electron microscope equipped with EDS (Energy-dispersive X-ray spectroscopy) analyser. The micro-Vickers hardness in the coated layer cross-section and the substrate were measured with an indentation load of 9.8 N and loading time of 15 s at room temperature. The wear behaviour of the laser cladded zone was evaluated using a pin-on-disk dry sliding wear tester in air at room temperatures. A stationary sample with a diameter of 2.5 mm was slid against a rotating disk with a rotational speed of 265 rpm for 15 min. The tests were carried out at a fixed load of 2 kg applied to the pin. Before the test, all the specimens were ground on emery paper up to # 600 to get smooth and flattened surface. The specimens were weighted before and after the test with a sensitive electronic balance with an accuracy of 0.001 g. The differences in average weight before and after the wear test were measured and accounted. Three specimens of each condition were chosen for wear tests. The untreated base metal was selected as the reference material for the wear test. The corrosion behavior of the substrate and the cladding layer were evaluated by the corrosion current density and the corrosion potential obtained from polarization curves in a 3 wt. % NaCl solution at room temperature with an IM-6 electrochemical workstation. The scanning potential can be in the range of -1.0 V to +2 V, and the scanning rate was 5 mV/s.

3. Results and discussion

3.1 Macro and micro-structure analysis

Fig. 1 shows the macrographs of the cross-sections of the surface laser treated layer at different processing powers. The treated layers in all conditions appeared as nearly half moon shape inside the Ti alloy substrate. This is may be due to the higher defocusing distance that penetrate the heat into deeper areas and increase the dilution of the cladding materials with the substrate. It was clear from these figures that the area of the cladding layer is in direct proportion to the laser power. At laser power of 2000 W, the cladding layer appeared as a deeper complete half moon above the substrate, while it appears as a narrow band at laser power of 1000 W. The dimensions of laser treated zones were 2.99 mm width and 0.52 mm depth for 1000 W, 3.05 mm width and 0.61 mm depth for 1500 W, and 3.1 mm width and 0.73 mm depth for 2000 W. This is due to the more heat input that produced at higher powers which melts the cladding materials together with more areas from the substrate. The microstructures of the cladding layer treated by power of 2000 W are shown in Figs. 2 and 4. Many (white color) fine long dendrites with short secondary arms were precipitated inside the Ti alloy as clearly shown in Fig. 2. EDS demonstrated that these dendrites were VC, as shown in Fig. 3(b), while the matrix was Ti alloy substrate, Fig. 3(a). This means that a surface composite consisted of Ti alloy reinforced with VC dendrites was produced in the cladded layer. In addition, the dendrite morphology of the high melting point VC particles means that they were melted and then solidified during the laser processing. As it is well known that laser technology is characterized by a high energy density and ceramics have a much higher capability to absorb laser energy than metals [26]. Therefore, VC particles were melted (or partially melted) in spite of its extremely high melting point, and then solidified by the self-quenching effect of the very high cooling rate after laser surface treatment.

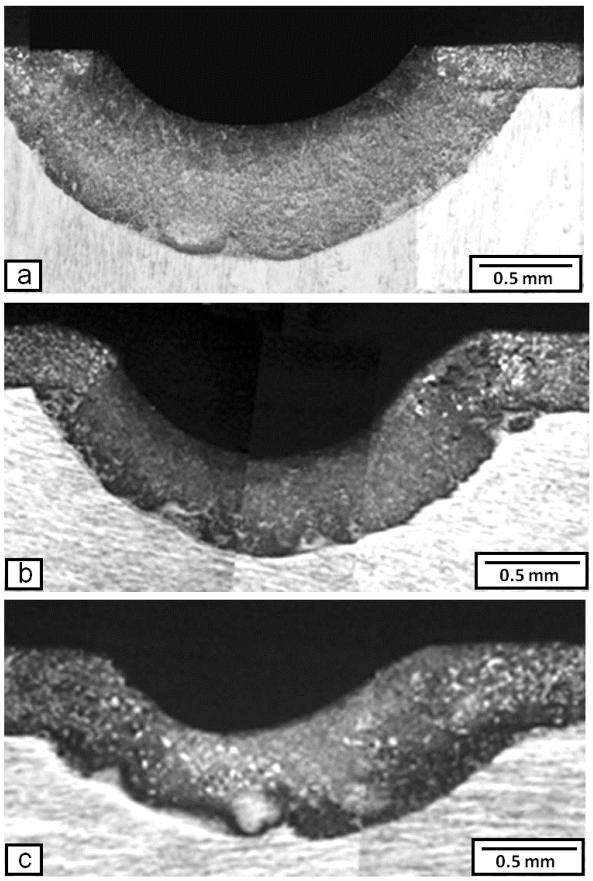

Fig. 1 Macro-views of the cross-sections of the surface laser cladding layer at different processing powers of 2000 W, 1500 W, and 1000 W

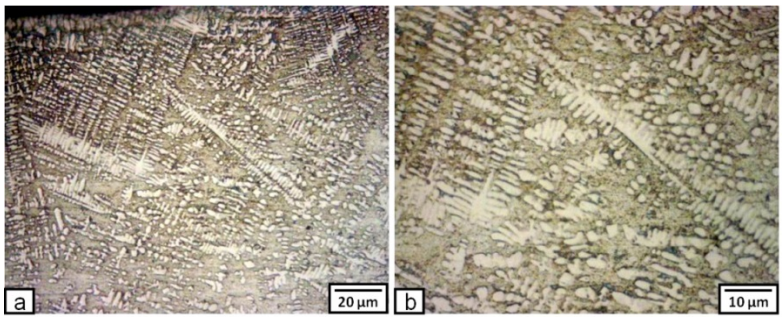

Fig. 2 Micrographs of the top portion of the laser cladding layer near the free surface produced by processing power of 2000 W

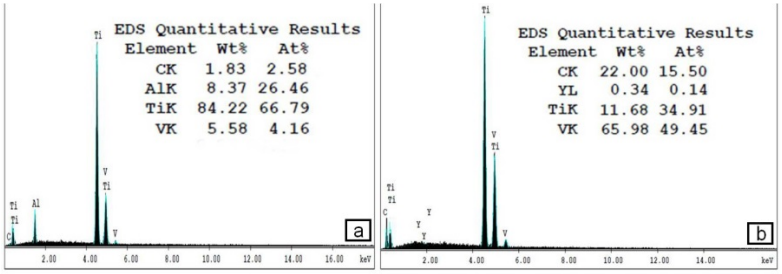

Fig. 3 EDS analysis of: (a) matrix, and (b) dendritic structure that appeared in the cladding layer produced at processing power of 2000 W

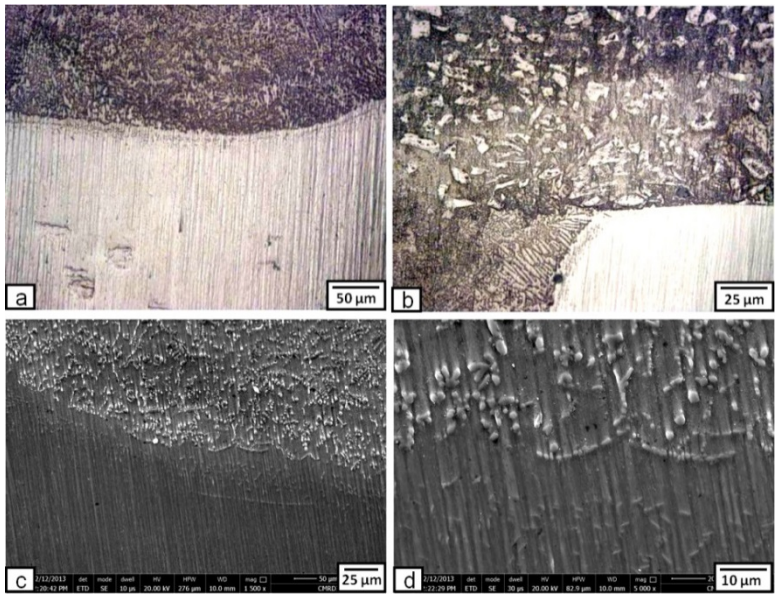

Fig. 4 Micrographs of the lower portion of the laser cladding layer produced by processing power of 2000 W showing the interface with the substrate

By going down through the cladding layer, near the interface, some fine VC particles are appeared distributed homogenously inside the Ti alloy matrix as shown in Fig. 4. In this area, the higher heat input melts the course VC particles. The relatively lower cooling rate at this embedded area was not fast enough to form VC dendrites. So, it appeared as fine VC particles. It is obviously to note here that the cladding layer was tightly bonded to the substrate without any defects as shown in Fig. 4.

At processing power of 1500 W, the amounts of VC dendrites are reduced and it concentrates at the top portion of the cladding layer (near the free surface) as shown in Figs. 5(a) and 5(b). The VC morphology is appeared as some dendrites mixed with particles. At the lower portion of

the cladding layer (near the interface), the VC particles appeared as their original course particles shape, as clearly shown in Figs. 5(c) and 5(d). The heat generated is not enough to melt most of the added VC particles. Most of the VC dendrites are concentrated at the top center of the cladding layer where the heat is concentrated.

When the laser processing power was reduced to 1000 W, the generated heat is not enough to melt the added VC particles. There was almost no dendritic VC morphology in the cladding layer produced at this condition as shown in Fig. 6. Moreover, the VC particles accumulated in clusters as shown in Fig. 6(c). The lower heat input at this condition reduces the dilution process of the VC particles in the Ti alloy matrix. This causes that the VC particles to concentrate in small area in their original shape.

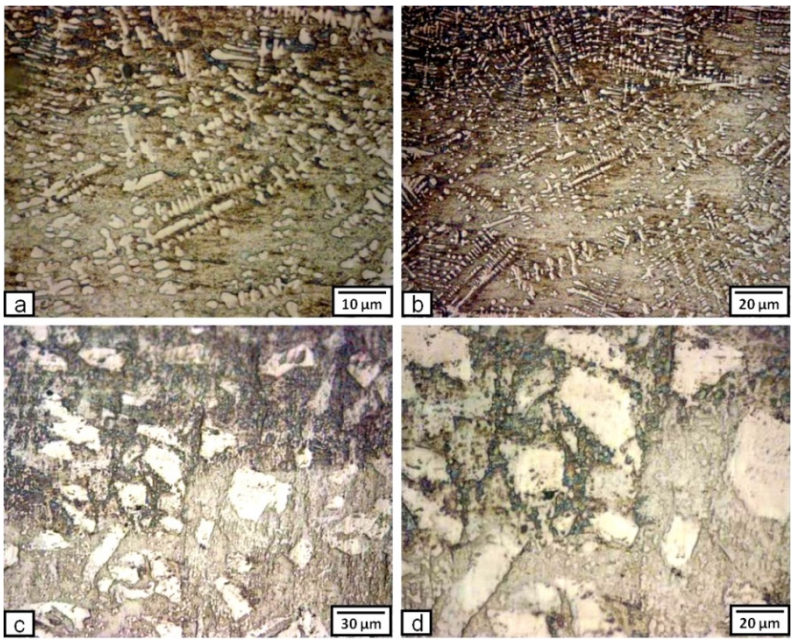

Fig. 5 Micrographs of the laser cladding layer produced by processing power of 1500 W: (a) and (b) – top portion near the free surface, (c) and (d) – lower portion

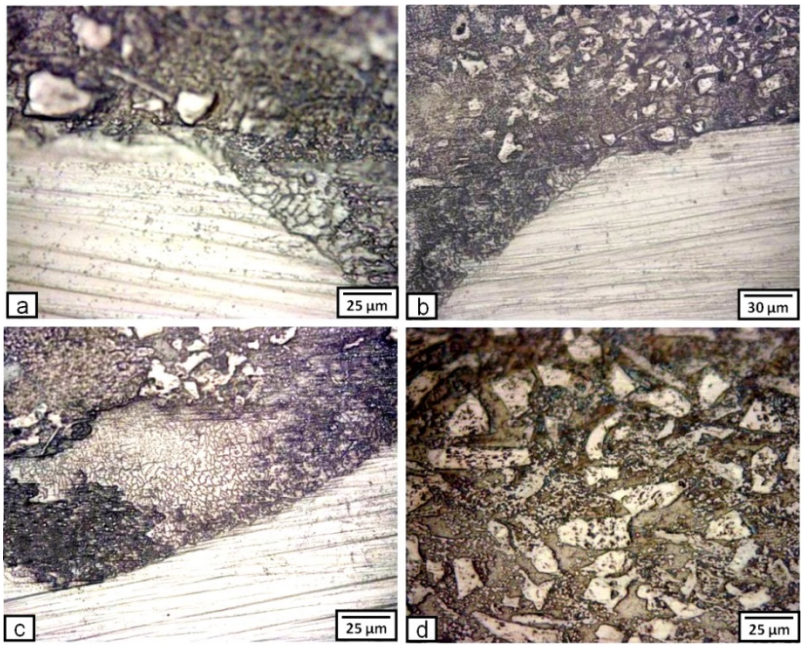

Fig. 6 Micrographs of the laser cladding layer produced by processing power of 1000 W: (a) – right side of the cladding layer, (b) – left side, (c) – lower center, (d) – center of the cladding layer

3.2 Surface and subsurface microhardness evaluation

Fig. 7 shows the hardness distribution along the depth direction of the laser-cladded areas at different powers. The substrate has an average microhardness value of approximately 360 HV. At all condition, high microhardness values (almost twice as the substrate) were obtained at the surface and a certain subsurface layer and decreased towards the substrate. This is due to the presence of hard VC particles with a great amount in these areas.

These results also indicate that the increase in processing power cause a decrease in the free surface hardness improvement and an increase in the hardened zone depth. The decrease in processing power decreases the amount of the heat input and consequently the dilution is decreased. As a result, the volume fractions of VC in the cladded layer are increased. This represents a main reason for the high hardness values resulted in case of the low processing power. Conversely, the increase of processing power increases the heat input and consequently the dilution is increased. As a result, the volume fractions of unmelted VC in the cladded layer are decreased. Moreover, during the re-solidification, some carbon came from the melted VC particles can be pushed by the solidification front due to it has low solubility in Ti [20, 21]. For that reason, the percentage of carbon in this region can be increased. This can be represents one of the main reasons for the high hardness at this region.

The hardness distributions at powers of 2000 W and 1500 W showed almost homogenous trend, which that at power of 1000 W showed inhomogeneous distribution. This may be due to the homogeneity of the VC particles inside the cladding layer, which confirm the microstructure analysis.

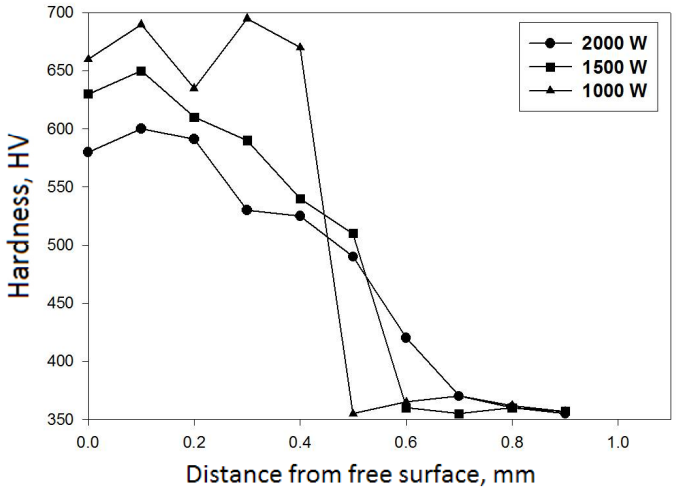

Fig. 7 Microhardness profiles through the depth of the laser treated zone obtained at different laser powers

3.3. Wear rate of the developed surface layer

The wear rates were calculated for the cladded layer and the substrate material as described in the experimental work. From Fig. 8 it is clear that the addition of VC powder on the Ti alloy substrate with the aid of laser improved the overall wear resistance of the MMC produced in the cladding zone on the surface. The three conditions of 2000 W, 1500 W, and 1000 W processing powers gave high reduction in wear rate. Generally, the improved wear resistance in the laser cladded zone can be mainly attributed to the higher hardness of this zone due to: i) the presence of VC in the form of refined particles and dendrites, ii) the carbon diffusion in the matrix and iii) the strong interface bonding between the Ti alloy matrix and the VC reinforcement. The hard reinforcing phase (VC) act as load-bearing compounds and resist the plastic deformation of the matrix phase. With the increase of power, the volume fraction of unmelted VC was decreased (due to the increase of dilution) and as a result the improvements in hardness and the wear resistance of the cladded zone were decreased. In the same time, the non-homogeneous distribu-

tion of VC particles inside the cladding layer at power of 1000 W increases the weight loss, and in consequence, reduces the wear resistance.

Regarding the corrosion resistance evaluation, the sample treated at processing power of 1500 W was chosen due to that it gave the best results regarding the dimensions, microstructure, hardness, and wear resistance of the resulted zone. Fig. 9 shows the polarization curves of Ti alloy substrate and the treated layer. From this figure, it is clear that the corrosion potential of the treated sample was shifted to more positive than that of the Ti alloy substrate. Also, the corrosion current of the treated layer showed lower values than that of the Ti alloy substrate. It is well known that when the potential is increased and the current is decreased, the polarization resistance is increased and the material show improved corrosion resistance. Thus, it is clearly evident that the laser melting of Ti alloy had a positive influence on its the corrosion behavior.

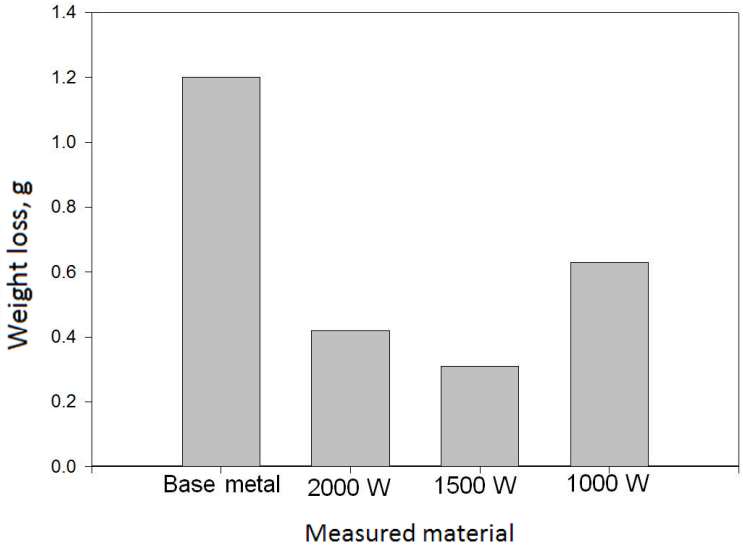

Fig. 8 Wear weight losses of untreated and laser cladded specimens with different laser powers

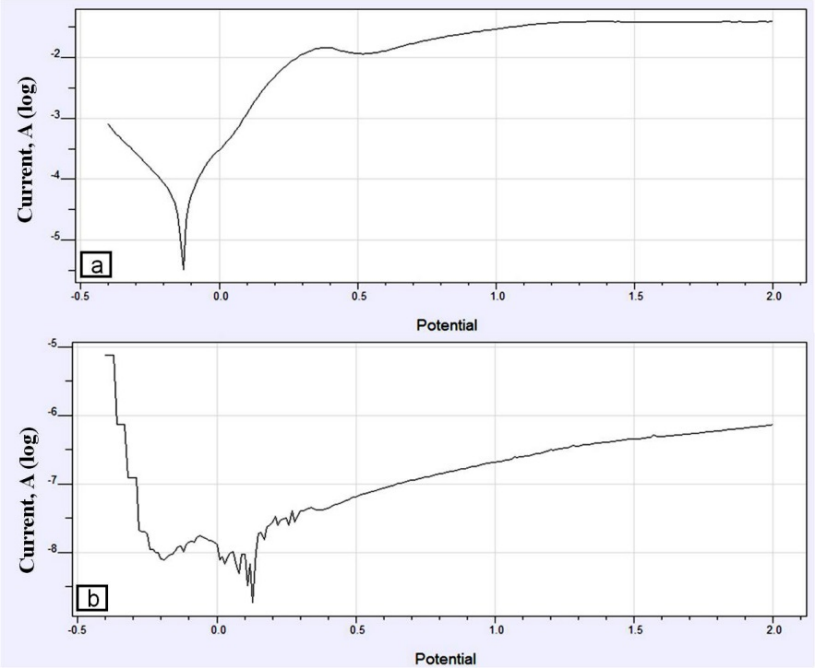

Fig. 9 Polarization curves of the substrate (a), and the cladding layer produced with processing power of 1500 W (b)

4. Conclusion

The surface of Ti-6Al-4V alloy was treated by laser cladding in argon atmosphere at processing powers of 2000 W, 1500 W, 1000 W, and fixed travelling speed of 4 mm/s. For this purpose, the YAG Fiber laser and VC powder as a cladding material with 30-40 μm particle size were used. The treated specimens were investigated in macro and microscopically scale using optical and scanning electron microscope. Surface and subsurface hardness, and wear and corrosion resistances were evaluated. The results of this work led to the following conclusions:

- Surface cladded layers of Ti-6Al-4V alloy metal matrix composite reinforced with VC particles were produced on Ti-6Al-4V alloy at all processing conditions. The size of the cladding layer is increased by increasing the processing power. The cladding layer was well bonded to the substrate, especially at higher processing powers.
- The VC particles were homogenously distributed within the cladding layer at processing powers of 2000 W and 1500 W, while it shows some clusters at power of 1000 W.
- Some of the VC particles were melted and re-solidified as fine long dendritic structure during the laser treatment.
- The cladding layer produced at all processing conditions resulted in remarkably improvement of hardness and wear resistance (almost twice). As the processing powers decreased, the surface of the cladding layers showed higher hardness. Higher laser power leads to a deeper hardened zone.
- The laser treated layer show improved corrosion resistance.
- The application of Ti-6Al-4V alloy can be widen by this surface treatment to include severe and harsh environment. Moreover, it can prolong their service life.

Acknowledgement

This work was supported by the King Abdel-Aziz City of Science and Technology (KACST) through the Science and Technology Center at King Khalid University (KKU), Project No. (10-ENE1161-07). The authors thank both KACST and KKU for their financial support. Special thanks to Prof. Ahmed Tahir, Vice President of KKU and Prof. Abdullah Al-Sehemi, Head of the Scientific Research at KKU for their support.

References

[1] Ochonogor, O.F., Meacock, C., Abdulwahab, M., Pityana, S., Popoola, A.P.I. (2012). Effects of Ti and TiC ceramic powder on laser-cladded Ti-6Al-4V in situ intermetallic composite, *Applied Surface Science*, Vol. 263, 591-596, doi: 10.1016/j.apsusc.2012.09.114.

[2] Lin, Y.-C., Lin, Y.-C. (2011). Microstructure and tribological performance of Ti-6Al-4V cladding with SiC powder, *Surface and Coatings Technology*, Vol. 205, No. 23-24, 5400-5405, doi: 10.1016/j.surfcoat.2011.06.001.

[3] Mahamood, R.M., Akinlabi, E.T., Shukla, M., Pityana, S. (2013). Scanning velocity influence on microstructure, microhardness and wear resistance performance of laser deposited Ti6Al4V/TiC composite, *Materials and Design*, Vol. 50, 656-666, doi: 10.1016/j.matdes.2013.03.049.

[4] Tian, Y.S., Chen, C.Z., Li, S.T., Huo, Q.H. (2005). Research progress on laser surface modification of titanium alloys, *Applied Surface Science*, Vol. 242, No. 1-2, 177-184, doi: 10.1016/j.apsusc.2004.08.011.

[5] Alabeedi, K.F., Abboud, J.H., Benyounis, K.Y. (2009). Microstructure and erosion resistance enhancement of nodular cast iron by laser melting, *Wear*, Vol. 266, No. 9-10, 925-933, doi: 10.1016/j.wear.2008.12.015.

[6] Heydarzadeh Sohi, M., Ebrahimi, M., Ghasemi, H.M., Shahripour, A. (2012). Microstructural study of surface melted and chromium surface alloyed ductile iron, *Applied Surface Science*, Vol. 258, No. 19, 7348-7353, doi: 10.1016/j.apsusc.2012.04.014.

[7] Benyounis, K.Y., Fakron, O.M.A., Abboud, J.H., Olabi, A.G., Hashmi, M.J.S. (2005). Surface melting of nodular cast iron by Nd-YAG laser and TIG, *Journal of Materials Processing Technology*, Vol. 170, No. 1-2, 127-132, doi: 10.1016/j.jmatprotec.2005.04.108.

[8] Vamsi Krishna, B., Misra, V.N., Mukherjee, P.S., Sharma, P. (2002). Microstructure and properties of flame sprayed tungsten carbide coatings, *International Journal of Refractory Metals and Hard Materials*, Vol. 20, No. 5-6, 355-374, doi: 10.1016/S0263-4368(02)00073-2.

[9] Hua, G., Huang, Y., Zhao, J., Wang, L., Tian, Z., Zhang, J., Zhang, Y. (2004). Plasma-sprayed ceramic coating by laser cladding of Al_2O_3 nano-particles, *The Chinese Journal of Nonferrous Metals*, Vol. 14, No. 2, 199-203.

[10] Zenker, R., Buchwalder, A., Rüthrich, K., Griesbach, W., Nagel, K. (2013). First results of a new duplex surface treatment for cast iron: electron beam remelting and plasma nitriding, *Surface and Coatings Technology*, Vol. 236, 58-62, doi: 10.1016/j.surfcoat.2013.06.118.
[11] Zhang, W.P., Liu, S. (2005). Microstructure of Fe-Ti-B composite coating prepared by laser cladding, *The Chinese Journal of Nonferrous Metals*, Vol. 15, No. 4, 558-564.
[12] Tian, Y.S., Chen, C.Z., Wang, D.Y., Wang, Z.L. (2004). Study on microstructures and mechanical properties of in-situ formed multiphase coatings produced by laser cladding of titanium alloy with silicon and graphite powders, *Chineese Journal of Lasers*, Vol. 31, No. 7, 879-882.
[13] Chehrghani, A., Torkamany, M.J., Hamedi, M.J. Sabbaghzadeh, J. (2012). Numerical modeling and experimental investigation of TiC formation on titanium surface pre-coated by graphite under pulsed laser irradiation, *Applied Surface Science*, Vol. 258, No. 6, 2068-2076, doi: 10.1016/j.apsusc.2011.04.064.
[14] Yasavol, N., Abdollah-zadeh, A., Ganjali, M., Alidokht, S.A. (2013). Microstructure and mechanical behavior of pulsed laser surface melted AISI D2 cold work tool steel, *Applied Surface Science*, Vol. 265, 653-662, doi: 10.1016/j.apsusc.2012.11.070.
[15] Yilbas, B.S., Patel, F., Karatas, C. (2013). Laser controlled melting of HSLA steel surface with presence of B_4C particles, *Applied Surface Science*, Vol. 282, 601-606, doi: 10.1016/j.apsusc.2013.06.018.
[16] Gadag, S.P., Srinivasan, M.N., Mordike, B.L. (1995). Effect of laser processing parameters on the structure of ductile iron, *Materials Science and Engineering: A*, Vol. 196, No. 1-2, 145-154, doi: 10.1016/0921-5093(94)09719-4.
[17] Vilar, R. (2014). 10.07 – Laser powder deposition, In: Hashmi, S. (ed.), *Comprehensive Materials Processing*, Vol. 10, Elsevier, 163-216, doi: 10.1016/ B978-0-08-096532-1.01005-0.
[18] Uematsu, Y., Kakiuchi, T., Tokaji, K., Nishigaki, K., Ogasawara, M. (2013). Effects of shot peening on fatigue behavior in high speed steel and cast iron with spheroidal vanadium carbides dispersed within martensitic-matrix microstructure, *Materials Science and Engineering: A*, Vol. 561, 386-93, doi: 10.1016/j.msea.2012.10.045.
[19] Pierson, H.O. (1996). *Handbook of refractory carbides and nitrides: properties, characteristics, processing and applications*, New Jersey, Noyes publications, USA.
[20] Li, Y., Li, G., Yang, D., Li, G. (2012). Microstructure evolution and mechanical properties in VC/SiC nanomultilayers, *Applied Surface Science*, Vol. 258, No. 24, 9856-9858, doi: 10.1016/j.apsusc.2012.06.042.
[21] Tjong, S.C., Haydn, C. (2004). Nanocrystalline materials and coatings, *Materials Science and Engineering: R: Reports*, Vol. 45, No. 1-2, 1-88, doi: 10.1016/j.mser.2004.07.001.
[22] Lugscheider, E., Knotek, O., Bobzin, K., Bärwulf, S. (2000). Tribological properties, phase generation and high temperature phase stability of tungsten- and vanadium-oxides deposited by reactive MSIP-PVD process for innovative lubrication applications, *Surface and Coatings Technology*, Vol. 133-134, 362-368, 10.1016/S0257-8972(00)00963-4.
[23] Frykholm, R., Andrén, H.-O. (2001). Development of the microstructure during gradient sintering of a cemented carbide, *Materials Chemistry and Physics*, Vol. 67, No. 1-3, 203-208, doi: 10.1016/S0254-0584(00)00440-5.
[24] Ye, F., Hojamberdiev, M., Xu, Y., Zhong, L., Zhao, N., Li, Y., Huang, X. (2013). Microstructure, microhardness and wear resistance of VC_p/Fe surface composites fabricated in situ, *Applied Surface Science*, Vol. 280, 297-303, doi: 10.1016/j.apsusc.2013.04.152.
[25] Hashe, N.G., Neethling, J.H., Berndt, P.R., Andrén, H.-O., Norgren, S. (2007). A comparison of the microstructures of WC-VC-TiC-Co and WC-VC-Co cemented carbides, *International Journal of Refractory Metals and Hard Materials*, Vol. 25, No. 3, 207-21, doi: 10.1016/j.ijrmhm.2006.05.001.
[26] Kąc, S., Kusiński, J. (2003). SEM and TEM microstructural investigation of high-speed tool steel after laser melting, *Materials Chemistry and Physics*, Vol. 81, No. 2-3, 510-512, doi: 10.1016/S0254-0584(03)00062-2.

APEM journal
Advances in Production Engineering & Management
Volume 9 | Number 4 | December 2014 | pp 168–180
http://dx.doi.org/10.14743/apem2014.4.185
ISSN 1854-6250
Journal home: apem-journal.org
Original scientific paper

Parametric study of die sinking EDM process on AISI H13 tool steel using statistical techniques

Bose, G.K.[a,*], **Mahapatra, K.K.**[b]

[a]Department of Mechanical Engineering , Haldia Institute of Technology, Haldia, India
[b]Technical Service, Central Institute of Plastic Engineering Technology, Bhubaneswar, India

ABSTRACT

The correct optimization of process parameters is one of the more important aspects when taking into consideration the majority of manufacturing processes and particularly for processes relating to electrical discharge machining (EDM). It is capable of machining geometrically complex or hard material components that are precise and difficult-to-machine, such as heat-treated tool steels, composites, super alloys, ceramics, carbides, heat resistant steels etc. The presented study focused on the electric discharge machining (EDM) of AISI H 13, W.-Nr. 1.2344 Grade: Orvar Supreme for finding out the effect of machining parameters such as discharge gap current (GI), pulse on time (POT), pulse off time (POF) and spark gap (SG) on performance responses such as material removal rate (MRR), surface roughness (R_a) and overcut (OC) using a square-shaped Cu tool with lateral flushing. A well-designed experimental scheme was used to reduce the total number of experiments. Parts of the experiment were conducted within the L27 orthogonal array based on the Taguchi method and significant process parameters were identified using analysis of variance (ANOVA). It was found that MRR is affected by gap current and R_a is affected by pulse on time. Moreover, the signal-to-noise ratios associated with the observed values in the experiments were determined by which factor was most affected by the responses of MRR, R_a and OC. These experimental data are investigated using response surface methodology (RSM) for the effects of four EDM parameters GI, POT, POF and SG on MRR, R_a and OC. Response surfaces and contour plots were considered for exploring the importance of the variables and their levels, so as to optimize the responses. Finally multi-response optimization was carried out by means of overlaid contour plots and desirability functions.

ARTICLE INFO

Keywords:
Die sinking EDM
Multi response optimization
Analysis of variance
Response surface methodology

**Corresponding author:*
gkbose@yahoo.com
(Bose, G.K.)

Article history:
Received 29 June 2014
Revised 4 November 2014
Accepted 10 November 2014

1. Introduction

Electro discharge machining (EDM) is an electro-thermal non-traditional machining process, where electrical energy is used to generate electrical spark and material removal mainly occurs due to thermal energy of the spark. The EDM process is employed widely for making tools, dies and other precision parts. It is capable of machining geometrically complex or hard material components, that are precise and difficult-to-machine such as heat treated tool steels, composites, super alloys, ceramics, carbides, heat resistant steels etc. In the Sinker EDM process, two metal parts submerged in an insulating liquid are connected to a source of current which is switched on and off automatically depending on the parameters set on the controller.

A brief literature review on EDM process is presented here. Selvakumar et al. [1] studied the experimental performance based on L-18 orthogonal array with pulse on time, pulse off time, peak current, wire tension, servo feed setting and corner angle as control factors. ANOVA was performed to find the significance of the factors considered. Kapoor et al. [2] investigated the effect of cryogenic treated brass wire electrode on surface roughness and material removal rate for WEDM. They described the influence of various machining parameters (including pulse width, time between two pulses, wire tension and wire feed) on surface roughness and material removal rate by using one variable at a time approach. Dvivedi et al. [3] investigated the EDM using Al 6063 SiCp metal matrix composite for surface quality. Aligiri [4] studied the real-time pulse discriminating system employed as the basic platform of micro-EDM control system for a more detailed interpretation of the state of micro-EDM process. Liu et al. [5] describes the use of adductive networks to monitor the electrical discharge machining (EDM) process. Ayesta et al. [6] studied parameters related to the discharge process (current, pulse time and servo voltage) on machining time and electrode wear in EDM process. Nipanikar [7] studied the cutting of D3 Steel material using EDM with a copper electrode by using Taguchi methodology. Salem et al. [8] predicted the surface roughness by experimental design methodology in EDM. Singh and Kalra [9] optimize the machining parameters of EDM on OHNS steel using the Taguchi method and ANOVA methods. Syed and Palaniyandi [10] has studied the performance of electrical discharge machining using Al powder suspended distilled water using Taguchi Design of Experiments. Kumar et al. [11] present an investigation on WEDM of pure titanium (grade-2) while determining surface roughness using multi response optimization. Kohli et al. [12] studied the machining of medium carbon steel (AISI 1040) using die sinking EDM with input parameters like discharge current (I_p), pulse on time (T_{on}), pulse off time (T_{off}). Mohanty et al. [13] presented a thermal-structural model to analyze the process parameters and their effect on responses like MRR, tool wear rate and residual stresses using EDM process. Arikatla et al. [14] studied the optimization of EDM using design of experiment. Baseri et al. [15] investigated the effects of the flushing types on rotary electro discharge machining performance using alloy steel of X210Cr12.

The objective of the work is to study the characteristic features of the EDM process as reflected through Taguchi design based experimental studies with various process parametric combinations like gap current (GI), pulse on time (POT), pulse off time (POF), and spark gap (SG) on material removal rate (MRR), surface roughness (R_a), and overcut (OC). The significant process parameters are identified using analysis of variance (ANOVA). These experimental data are further investigated using response surface methodology (RSM). The present paper is aimed at fulfillment of two basic but conflicting objectives concurrently higher material removal rate (MRR) and lower surface roughness (R_a) by employing a single set of optimal or near optimal process variables following response surface methodology (RSM). Response surfaces and contour plots are studied to investigate the prominence of the variables and their levels so as to optimize the responses. Finally multi-response optimization is carried out using overlaid contour plots and desirability functions.

2. Planning for experimentation

In the present research work electric discharge machine (ACTSPARK SP1, China) die-sinking type with servo-head (constant gap) and positive polarity for electrode is used for experimentation. Commercial grade EDM-30 oil (specific gravity of 0.80 at 25 ˚C, viscosity of 3.11×10^{-6} m^2s^{-1} at 38 ˚C) was used as dielectric fluid. With external lateral flushing using a square-shaped Cu tool (12 mm ×12 mm) having a pressure 0.2 kgf/cm^2 is used. Experiments were conducted with positive polarity of electrode. AISI H-13 Tool steel work piece material is selected for the experiment. The pulsed discharge current was applied in various steps in positive mode. The EDM set-up consists of dielectric reservoir, pump and circulation system, power generator and control unit, working tank with work holding device, *X*-*Y* table accommodating the working table, tool holder and the servo system to feed the tool part. The servo control unit is provided to maintain the pre-determined gap. It senses the gap voltage and compares it with the present value and the different in voltage is then used to control the movement of servo motor to adjust the gap. The

MRR is expressed as the ratio of the volume of the work piece material removed during machining the cavity to the machining time. Surface roughness of the cavity surface is expressed as R_a (μm) and measured using stylus type profilometer named Talysurf (Taylor's Hobson Surtronic 3+). Overcut is expressed as half the difference of area of the cavity produced to the tool frontal area. Area of cavity and frontal area of electrode can be calculated by measuring the respective length and width using Toolmaker's microscope.

When performing an experiment, varying the levels of the factors simultaneously rather than one at a time is efficient in terms of time and cost, and also allows for the study of interactions between the factors. Based on past research works and preliminary investigation, four parameters were chosen as input. Initially L9 orthogonal array is employed for the experimentation. The input parameters were varied with three levels in nine experimental run. There are other factors which may affect the measured performance like duty cycle, flushing pressure, lift time etc., however, were kept constant during experimentation. Table 1 exhibits the different levels of control parameters during machining process.

Table 1 Parametric settings and responses for experimental run

	Control parameters				Responses		
Expt. No.	POT (μs)	POF (μs)	GI (A)	SG (mm)	MRR (mm^3/s)	R_a (μm)	OC (mm^2)
1	16	12	7	0.16	0.0346	9.6	4.237
2	16	16	9	0.18	0.0933	10.733	2.358
3	16	20	11	0.2	0.1441	11.133	3.556
4	20	12	9	0.2	0.1581	7.6	4.469
5	20	16	11	0.16	0.2064	9.4	4.349
6	20	20	7	0.18	0.0133	6.6	3.376
7	24	12	11	0.18	0.1267	7.93	3.241
8	24	16	7	0.2	0.0085	3.467	3.124
9	24	20	9	0.16	0.0943	9.2	4.876

3. Results analysis using ANOVA

ANOVA is a functional method for estimating error variance and determining the relative importance of various process variables [16]. The experimental outcomes are explored to study the role of different process variables on various responses by using S/N ratio and ANOVA. The result analysis is carried out by statistical software MINITAB, version 13.

S/N ratio determines the contribution of different process variables on various responses. The goal is to find out an optimal combination of control factor settings that achieve robustness against (insensitivity to) noise factors. S/N ratio analysis for MRR (mm^3/min) is carried out on the basis of larger is the better and the corresponding S/N ratio is expressed as follows:

$$n_1 = -10\log_{10}\left(\frac{1}{n}\sum_{i=1}^{n}\frac{1}{MRR^2}\right) \quad (1)$$

S/N ratio analysis for R_a is modeled on the basis of smaller is the better and corresponding equation is

$$n_2 = -10\log_{10}\left(\frac{1}{n}\sum_{i=1}^{n}R_a^2\right) \quad (2)$$

S/N ratio analysis for OC is modeled on the basis of smaller is the better and corresponding equation is

$$n_3 = -10\log_{10}\left(\frac{1}{n}\sum_{i=1}^{n}OC^2\right) \quad (3)$$

The S/N plot for MRR, R_a and overcut are shown in Fig. 1.

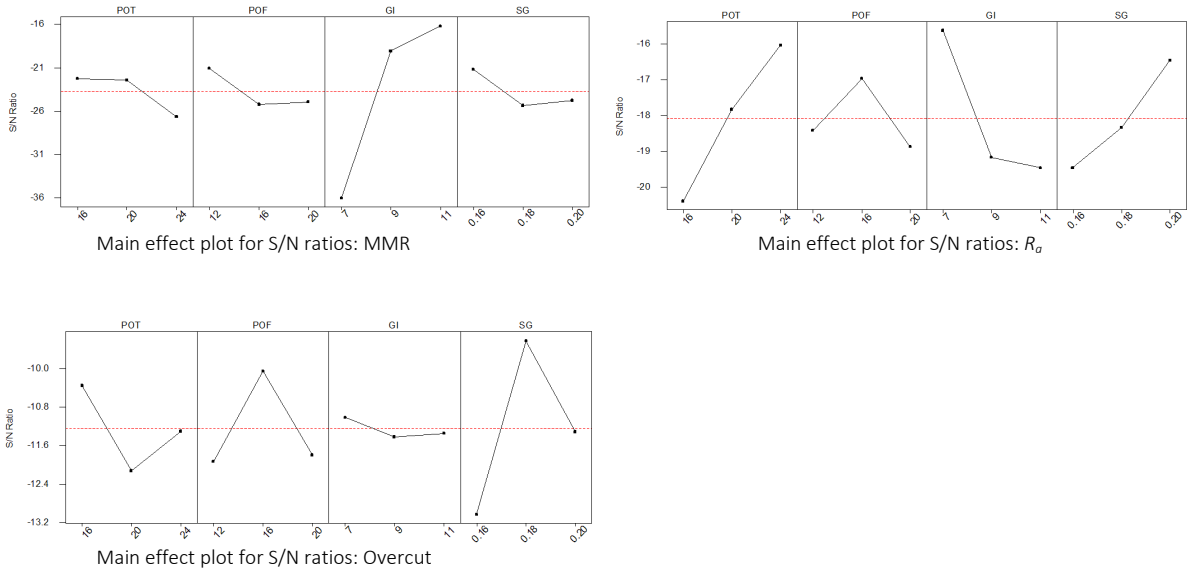

Fig. 1 S/N ratio plot for MRR, R_a, and overcut

It is observed from the S/N ratio graph that the MRR attains its peak with the parametric combination of POT (16 μs), POF (12 μs), GI (11 A), SG (0.16 mm). For smaller is better for R_a is obtained at POT (24 μs), POF (16 μs), GI (7 A), SG (0.20 mm). Similarly for smaller is better for OC is obtained at POT (16 μs), POF (16 μs), GI (7 A), SG (0.18 mm).

ANOVA results as exhibited from F-values and percentage contribution of the process variables states that the F-values of gap current assume value 22.337 with a yield of 82.28 % in case of MRR. This implies that the variable have significant effects on MRR. Whereas in case of R_a, pulse on time (POT) alone is the major contributor having F-value of healthy 5.34 and having percentage contribution of 47.24 %, which is widely followed by gap current having F-value of approximately 4. Finally in case of overcut the spark gap (SG) alone is the major contributor having F-value of healthy 4.0 with percentage contribution of 65.60 %. Other factors here remain insignificant.

4. Results analysis using response surface methodology (RSM)

The response surface (output) can be related with the number of controllable variables $x_1, x_2, \ldots, x_k$ as

$$y = f(x_1, x_2, \ldots, x_k) + \varepsilon \tag{4}$$

A second order model is used to establish input-output relationship efficiently that takes the generic form

$$y = \beta_0 + \sum_{i=1}^{k} \beta_i x_i + \sum_{i=1}^{k} \beta_{ii} x_i^2 + \sum_{i=1}^{k} \beta_{ij} x_i x_j + \varepsilon \tag{5}$$

The predicted response for the model is

$$\hat{y} = \hat{\beta}_0 + \sum_{i=1}^{k} \hat{\beta}_i x_i + \sum_{i=1}^{k} \hat{\beta}_{ii} x_i^2 + \sum_{i=1}^{k} \hat{\beta}_{ij} x_i x_j \tag{6}$$

In the present work, Box-Behenken design is followed which is based on 2^k (k = 4) factorials with incomplete designs and found to be very efficient [17]. The process variables combinations and the corresponding responses are presented in Table 2.

Table 2 Combination of factors and responses for RSM

Expt. No.	POT (μs)	POF (μs)	GI (A)	SG (mm)	MRR (mm^3/s)	R_a (μm)	Overcut (mm^2)
1	20	12	11	0.18	1.2578	9.467	2.529
2	24	20	9	0.18	0.1572	2.067	3.498
3	24	16	11	0.18	0.832	7.6	5.3177
4	20	20	7	0.18	0.0956	2.267	2.7668
5	16	16	11	0.18	2.0271	9.067	2.892
6	20	16	7	0.16	0.07652	5.467	3.739
7	16	20	9	0.18	0.4193	7.733	4.9574
8	20	20	11	0.18	1.1941	11.367	5.6864
9	20	16	11	0.2	1.6	12.667	5.2014
10	24	16	9	0.16	0.0969	3.067	3.4982
11	20	16	9	0.18	0.0479	11.467	3.2556
12	16	16	7	0.18	0.0367	8.133	2.166
13	20	12	9	0.2	0.1581	7.6	4.4686
14	16	16	9	0.16	0.17158	8.867	3.376
15	20	16	9	0.18	0.1383	8.867	4.5915
16	20	16	11	0.16	0.2064	9.4	4.3488
17	20	20	9	0.16	0.08905	9.467	2.2852
18	20	16	9	0.18	0.095	8.667	3.2536
19	20	20	9	0.2	0.0771	9.333	5.4462
20	20	12	9	0.16	0.0773	9.333	1.4424
21	20	16	7	0.2	0.00877	8	1.6827
22	16	16	9	0.2	0.0892	11.6	2.8896
23	16	12	9	0.18	0.17357	9.867	2.0444
24	24	12	9	0.18	0.0324	3.933	1.9248
25	24	16	9	0.2	0.116	11.733	3.6187
26	24	16	7	0.18	0.00636	5.333	3.498
27	20	12	7	0.18	0.01333	6.6	3.376

4.1 Analysis of test results for material removal rate (MRR)

The estimated regression surface equation for MRR is:

$$\text{MRR} = -2.59 - 0.0349\ \text{POT} + 0.0032\ \text{POF} + 0.287\ \text{GI} + 5.55\ \text{SG} \tag{7}$$

The details of the regression analysis result are presented in Table 3. R-square as well as R-square (adjusted) assumes a value of 90.9 % and 80.2 %, respectively, that implies the model is poised to explain 90.9 % variability with process variable POT, POF, GI and SG . From the T values of the process variables it can be concluded that GI is the most significant process variables followed by SG, POF and POT.

Table 3 Estimated regression coefficients for material removal rate (MRR)

Term	Coef.	SE Coef.	T	P
Constant	0.0937	0.13894	0.675	0.513
POT	-0.1397	0.06947	-2.011	0.067
POF	0.0129	0.06947	0.186	0.855
GI	0.5733	0.06947	8.253	0.000
SG	0.1110	0.06947	1.597	0.136
POT*POT	0.0974	0.10421	0.935	0.368
POF*POF	0.0457	0.10421	0.439	0.669
GI*GI	0.4970	0.10421	4.769	0.000
SG*SG	-0.0765	0.10421	-0.734	0.477
POT*POF	-0.0302	0.12033	-0.251	0.806
POT*GI	-0.2912	0.12033	-2.420	0.032
POT*SG	0.0254	0.12033	0.211	0.837
POF*GI	0.0046	0.12033	0.039	0.970
POF*SG	-0.0232	0.12033	-0.193	0.850
GI*SG	0.3653	0.12033	3.036	0.010
Notes: S = 0.2407 R-Sq = 90.9 % R-Sq(adj) = 80.2 %				

The response surface plots of MRR with respect to GI, SG, POT and POF are shown in Fig. 2. It is observed that high levels of the two variables out of four yield maximum responses. The GI and SG have the significant effect on MRR. Since the response is proportional to the variables, there can not have any stationary point as evident from the surface plots. Further, the effect of GI is more pronounced than other three parameters. It is observed that high levels of the two variables out of four yield maximum responses. The GI and SG have the significant effect on MRR. Since the response is proportional to the variables, there can not have any stationary point as evident from the surface plots. Further, the effect of GI is more pronounced than other three parameters.

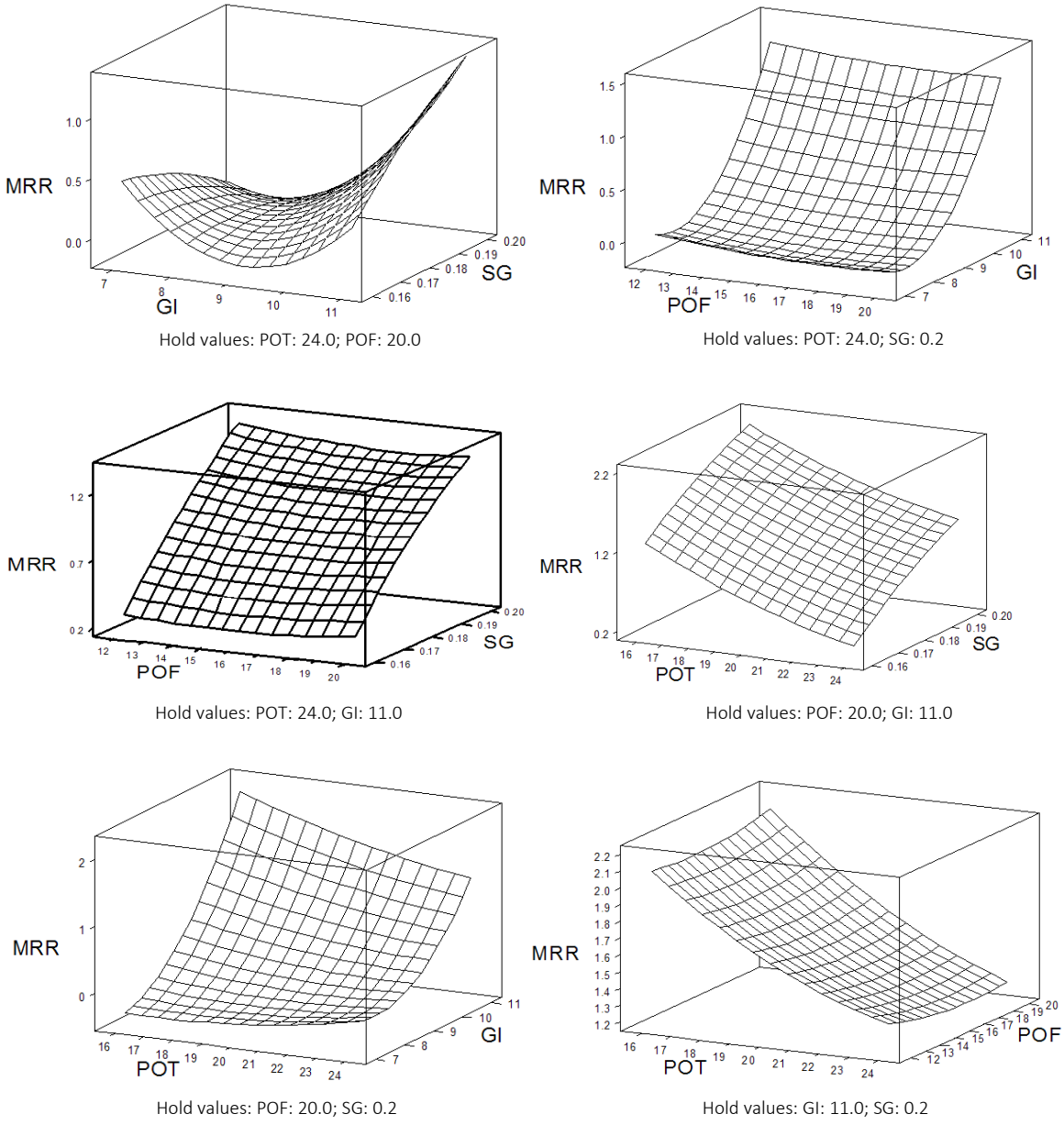

Fig. 2 Wire frame surface plot for MRR

4.2 Analysis of test results for surface roughness (R_a)

The estimated regression surface equation for R_a is:

$$\mathrm{RA} = -4.70 - 0.449\ \mathrm{POT} + 0.085\ \mathrm{POF} + 0.990\ \mathrm{GI} + 63.9\ \mathrm{SG} \tag{8}$$

The particulars of the regression analysis outcome are presented in Table 4. R-square as well as R-square (adjusted) furnishes a value of 71.4 % and 38.0 %, respectively, that implies the

model is balanced to explain 71 % variability with process variable POT, POF, GI and SG. From the T values of the process variables, it can be concluded that GI is the most significant process variables followed by SG, POF and POT.

The response surface plots of R_a with respect to GI, SG, POT and POF are shown in Fig. 3. It is seen that high levels of the two variables out of four capitulate utmost responses. The GI and SG have the considerable effect on R_a. Since the response is proportional to the variables, there can not have any stationary point as evident from the surface plots. Further, the effect of GI is more pronounced than other three parameters.

Table 4 Estimated regression coefficients for surface roughness (R_a)

Term	Coef.	SE Coef.	T	P
Constant	9.667	1.3010	7.430	0.000
POT	-1.795	0.6505	-2.759	0.017
POF	0.342	0.6505	0.525	0.609
GI	1.981	0.6505	3.045	0.010
SG	1.278	0.6505	1.964	0.073
POT*POT	-1.624	0.9758	-1.664	0.122
POF*POF	-1.620	0.9758	-1.660	0.123
GI*GI	-0.828	0.9758	-0.848	0.413
SG*SG	0.568	0.9758	0.582	0.571
POT*POF	0.067	1.1267	0.059	0.954
POT*GI	0.333	1.1267	0.296	0.772
POT*SG	1.483	1.1267	1.316	0.213
POF*GI	-0.608	1.1267	-0.540	0.599
POF*SG	0.400	1.1267	0.355	0.729
GI*SG	0.184	1.1267	0.163	0.873

Notes: S = 2.253 R-Sq = 71.4 % R-Sq(adj) = 38.0 %

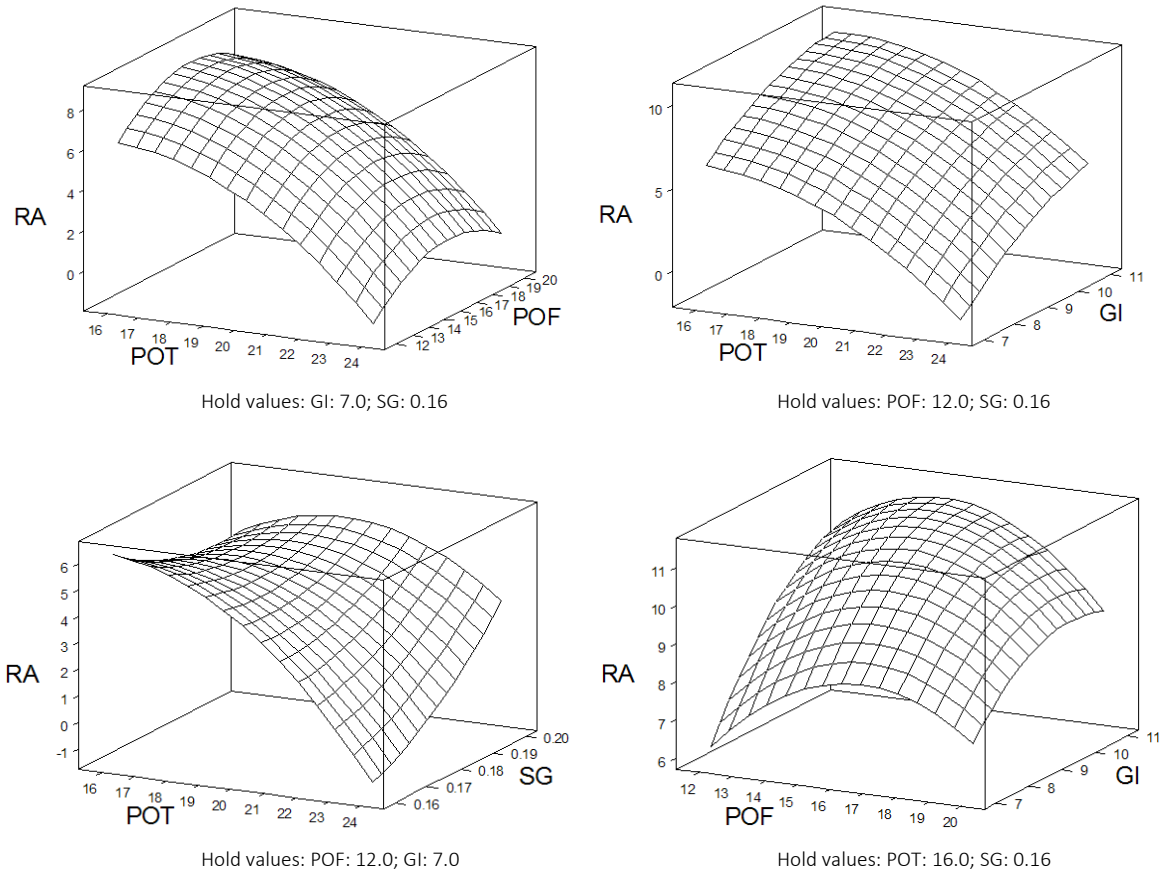

Fig. 3 Wire frame surface plot for R_a

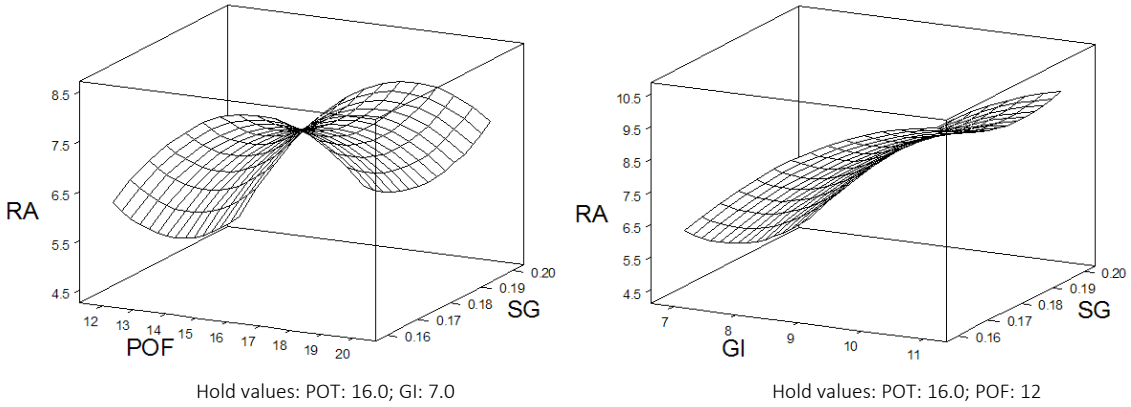

Fig. 3 Wire frame surface plot for R_a (continuation)

4.3 Analysis of test results for overcut (OC)

The estimated regression surface equation for overcut (OC) is:

$$OC = -4.70 - 0.449\ POT + 0.085\ POF + 0.990\ GI + 63.9\ SG \quad (9)$$

The particulars of the regression analysis are presented in Table 5. R-square furnishes a value of 61.4 % that implies the model is balanced to explain 61 % variability with process variable POT, POF, GI and SG. From the T values of the process variables, it can be concluded that POF is the most significant process variables followed by GI, SG and POT.

Table 5 Estimated regression coefficients for overcut (OC)

Term	Coef.	SE Coef.	T	P
Constant	3.7002	0.6344	5.833	0.000
POT	0.2525	0.3172	0.796	0.441
POF	0.8394	0.3172	2.646	0.021
GI	0.7289	0.3172	2.298	0.040
SG	0.3848	0.3172	1.213	0.248
POT*POT	-0.3339	0.4758	-0.702	0.496
POF*POF	-0.2409	0.4758	-0.506	0.622
GI*GI	0.1065	0.4758	0.224	0.827
SG*SG	-0.0444	0.4758	-0.093	0.927
POT*POF	-0.3350	0.5494	-0.610	0.553
POT*GI	0.2734	0.5494	0.498	0.628
POT*SG	0.1517	0.5494	0.276	0.787
POF*GI	0.6371	0.5494	1.160	0.269
POF*SG	0.0337	0.5494	0.061	0.952
GI*SG	0.7272	0.5494	1.324	0.210
Notes: S = 1.099 R-Sq = 61.4 % R-Sq(adj) = 16.4 %				

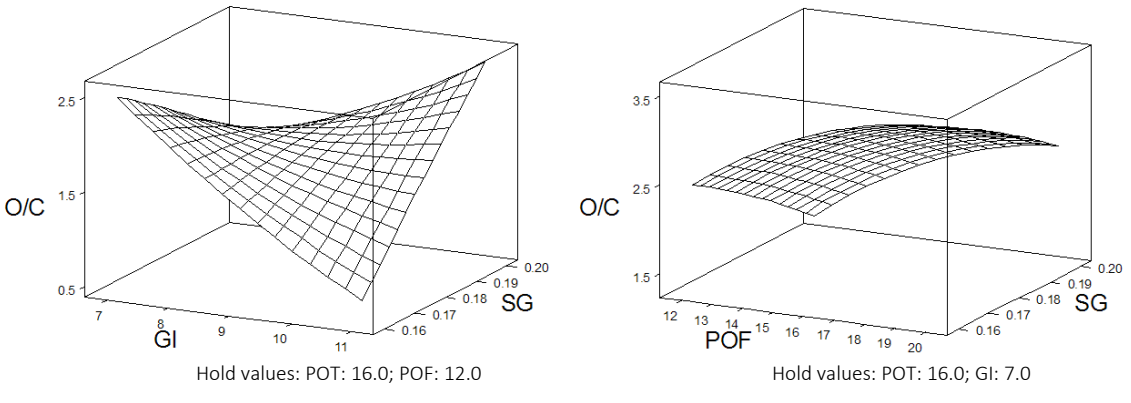

Fig. 4 Wire frame surface plot for overcut

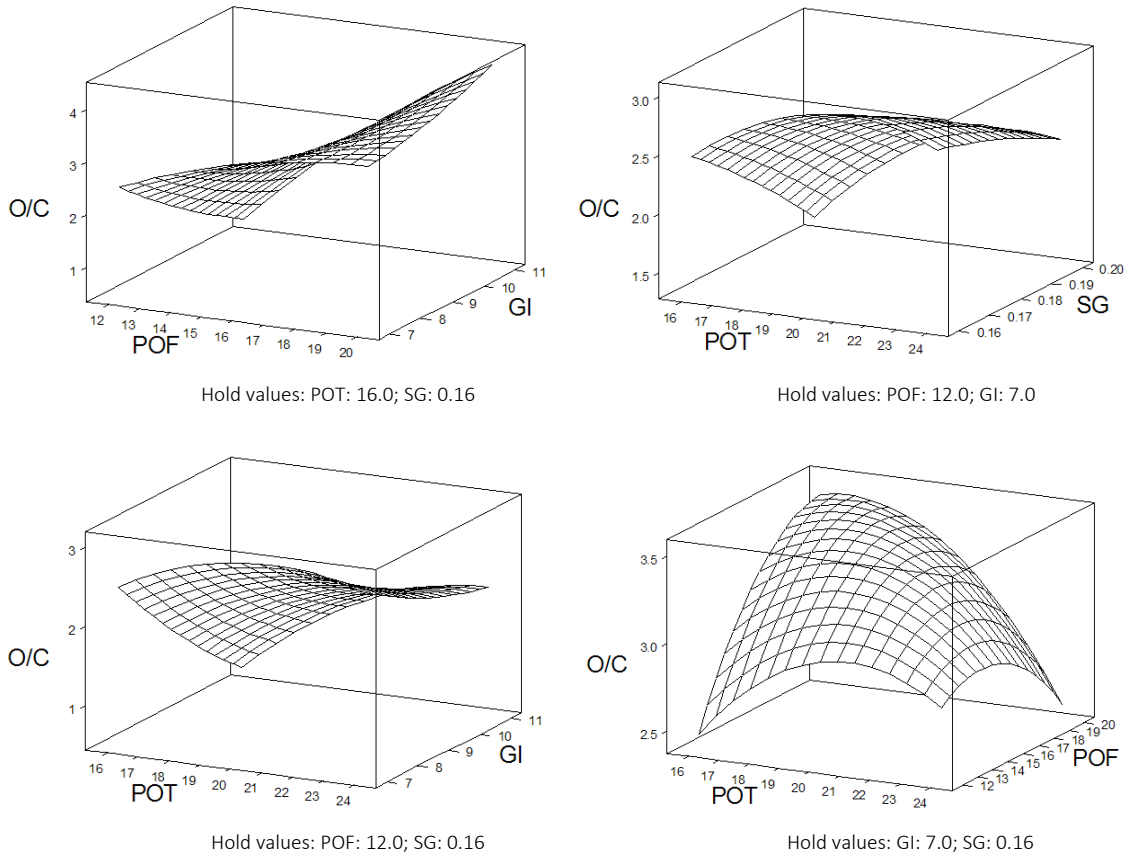

Fig. 4 Wire frame surface plot for overcut (continuation)

The response surface plots of R_a with respect to GI, SG, POT and POF are shown in Fig. 4. It is seen that high levels of the two variables out of four capitulate utmost responses. Since the response is proportional to the variables, there can not have any stationary point as evident from the surface plots. It is observed that the two variables out of four yield maximum responses. It clears that the POF and GI are the significant parameter for O/C.

5. Multi response optimization

5.1 Overlaid contour plots

High MRR and low R_a are the two major attributes of EDM machining process. These two responses are conflicting in nature and hence achieving the both simultaneously by a set of optimum variables combination is difficult. In this section the multi response optimization is conceded out so that two conflicting goals are fulfilled concurrently. We resort to overlay contour plots which are comparatively simple approach to review the levels of operating parameters that satisfy two constrained objectives. It is considered that R_a in the range of 1.067 μm to 5 μm found to be reasonably good and acceptable for most of the applications. MRR has been set between a lower bound of 0.1 mm^3/min and upper bound of 2.0 mm^3/min. Thus constrained equation become:

$$1.067 < R_a < 5.0 \tag{10}$$

$$0.1 < \text{MRR} < 2.0 \tag{11}$$

The overlaid contour plots of MRR and R_a is shown in Fig. 5.

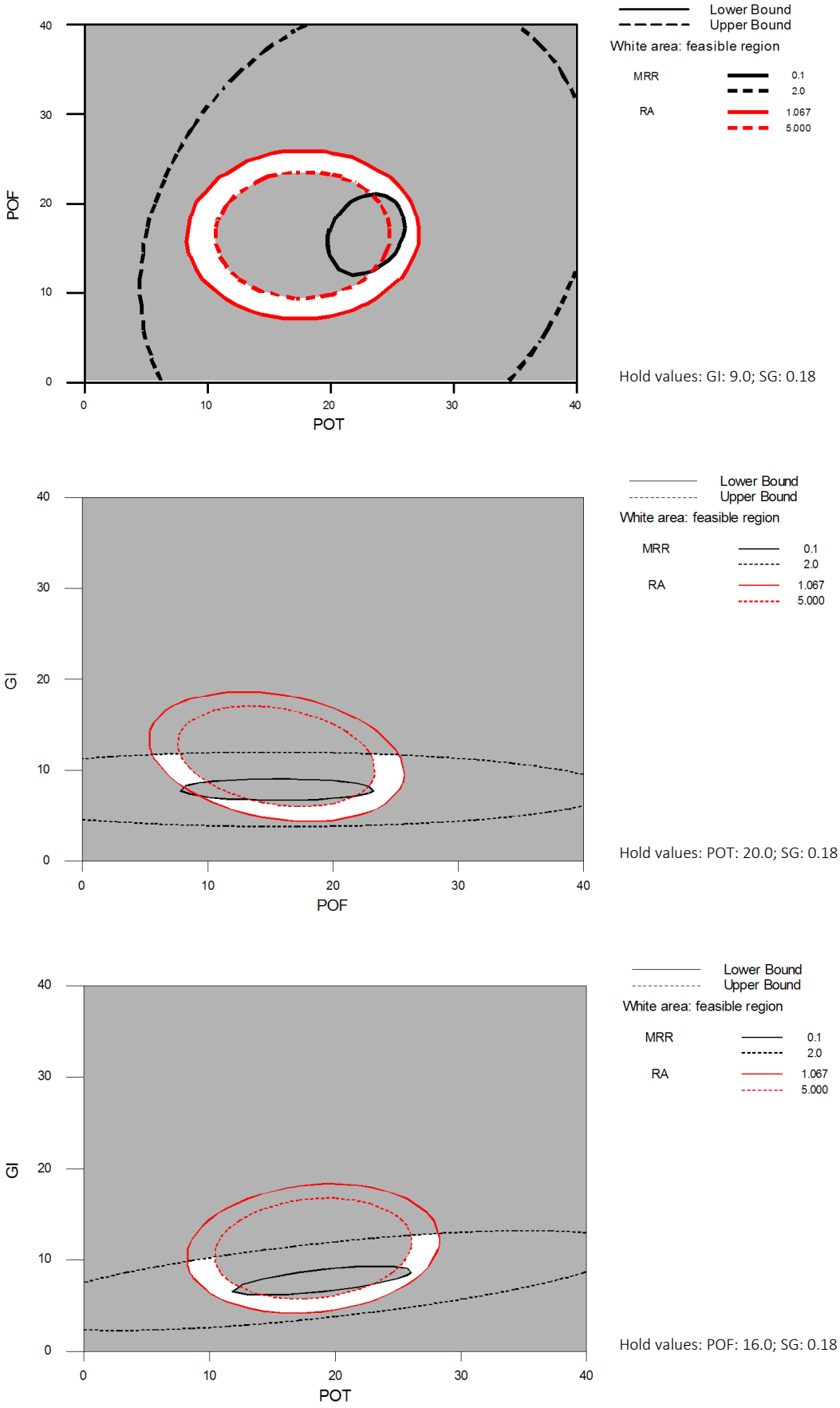

Fig. 5 Overlaid contour plot for MRR and R_a

The overlaid contour plot of MRR and R_a with respect to POT, POF, and GI are portrayed. The bounded white areas (unshaded) as indicated in the figure are the region that simultaneously satisfies global objectives along with possible combinations of process variables. The plots advocate that combination of moderate POT and medium POF help achieve the targets. Corresponding value of GI and POF can be predicted from the curve with the hold value of POT and SG. The white area in the figure highlights for optimum MRR and R_a and corresponding value of GI and POT can be predicted from the curve with the hold value of POF and SG.

5.2 Desirability functions

Response optimizer helps to help recognize the factor settings that optimize a single response or a set of responses. For multiple responses, the necessities for all the responses in the set must be fulfilled. Response optimization is frequently helpful in product development when it is required to establish operating conditions that will effect in a product with desirable properties. Here the goal, lower, target, upper, and weight characterize the desirability function for each individual response. The importance (Import) parameters decide how the desirability functions are combined into a single composite desirability. The response optimization is shown in Table 6.

From the S/N ratio plot of Taguchi design we get highest MRR at combination of POT (16 µs), POF (12 µs), GI (11 A), SG (0.16 mm) and lowest R_a at combination of POT (24 µs), POF (16 µs), GI (7 A), SG (0.2 mm). Hence an optimized combination of POT (20 µs), POF (16 µs), GI (9 A), SG (0.18 mm) can be taken as starting point.

Table 6 Desirability function results

Parameters	Goal	Lower	Target	Upper	Weight	Import
MRR	Maximum	0.100	0.5	2	1	1
R_a	Minimum	1.067	3.0	5	1	1

Predicted responses	**Global solution**
MRR = 0.34789, desirability is 0.61972 (61.972 %)	POT = 22.0652
R_a = 3.00017, desirability is 0.99992 (99.9992 %)	POF = 20.0000
Composite desirability is 0.78719 (78.719 %)	GI = 7.0000
	SG = 0.1600

Fig. 6 represents the optimization plot of the responses (MRR and R_a) with the process variables. It shows how the factors affect the predicted responses and allows to modify the factor settings interactively.

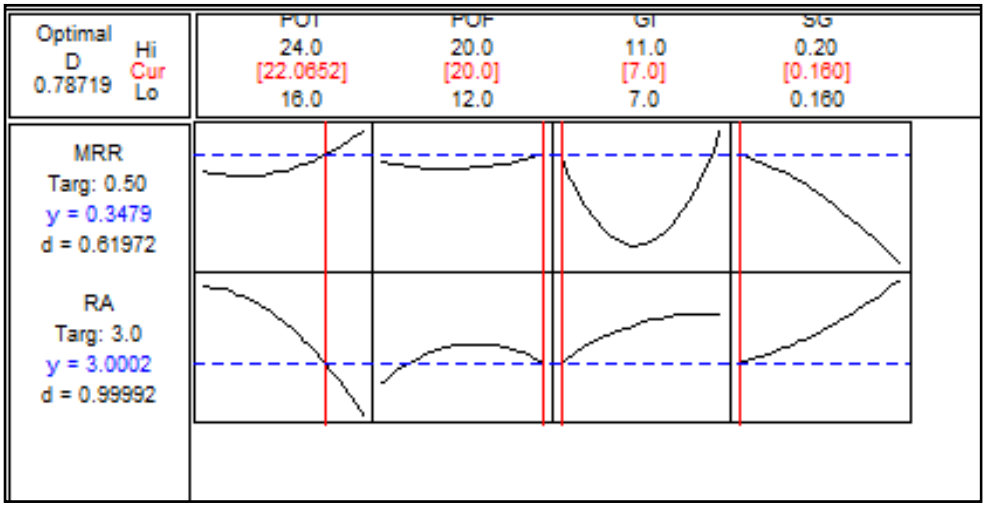

Fig. 6 Plot showing responses (MRR and R_a) against process variables

The figure shows the goal for the response, the predicted response, *y*, at the current factor settings, and the individual desirability score. The composite desirability, *D*, is displayed in the upper left corner of the graph. The label above the composite desirability refers to the current setting. When the optimization plot is created, the label is optimal. The vertical red lines on the graph represent the current factor settings. The horizontal dotted blue lines represent the current response values. From the earlier limit of MRR and R_a and assigning unbiased weight to the dual responses, the desirability of MRR becomes 0.91672 having predicted response of 0.34892 mm^3/min. The same for R_a is d_{Ra} = 0.99992 with the predicted response of 3.00017 μm. Finally the dual desirability is 0.78719 having POT = 2.0652, POF =20.0000, GI = 7.0000, SG = 0.1600 is the near optimal combination.

6. Discussion and conclusion

The experimental study indicates that in while machining AISI H13 tool steel using die sinking EDM process the responses are dependent on pulse on time, pulse off time, gap current and spark gap. The S/N ratio analysis along with ANOVA is a simple method to ascertain implication of several input parameters that administers multiple responses of the process. For higher MRR, GI is the most significant parameter and having contribution of 82.28 %. MRR increases with respect to increase of GI. In case of lower R_a, the POT is having the most significant effect and contributes 47.24 %. R_a decreases with the increase of POT and however R_a increases with increase of GI. For smaller overcut, SG is the most significant parameter and contributed 65.6 % and OC decreases with the increase of SG initially up to 0.18 mm then it increases with respect to SG.

The present work is carried out with a view to optimize MRR (maximize) and R_a (minimize) concurrently by employing a near optimal set of process variables. Since the optimization is carried out for a single pass machining, the due importance is given to the surface finish considering quality characteristics in a cost effective manner (enhanced productivity harnessing high MRR). This optimization is carried out by RSM that is promised to offer near optimal solution with little effort. The regression models are found to be worthy to express input-output relationship with a very high degree of predictability. The inferences drawn from the regression analysis is accentuated with the desirability functions. Gap current is found to be the most significant in comparison to the responses. The near optimal combinations of process variables are high POT, POF and low GI and SG to satisfy both the responses (MRR and R_a) simultaneously. This set of inputs can be used to further optimize other functions like machining cost and can form the backbone of adaptive control strategies (adaptive control with optimization and geometric adaptive control). The overlaid contour plot is a good visual aid to identify the feasible region in regard to a set of input variables.

The individual desirability for each predicted responses are calculated. The individual desirability values are then combined into the composite desirability. The closer the predicted responses are to your target requirements, the closer the desirability will be to 1. The composite desirability combines the individual desirability into an overall value, and reflects the relative importance of the responses. The higher the desirability the closer it will be to 1. Here MRR has an intermediate desirability score of 0.61972 because the predicted response for MRR of 0.34789 is approximately two-thirds of the way between the target of 2 and the lower bound of 0.100. The goal for MRR was to maximize; therefore higher values are more desirable. Similarly R_a has a desirability score of 0.9999 because the predicted response of 3 is nearer to the target of 3. The experiment was less successful optimizing overcut than MRR and R_a, respectively. The composite desirability of 0.78719 places greater emphasis on MRR (importance is 2) than on R_a and uvercut (importance is 1).

The RSM being a powerful tool, its potential can be extended to other areas of machining such as tool life, power and cutting force modeling. The experimental investigation for evaluating the optimal parametric combination and the subsequent effect of the parameters over the responses can act as an efficient and useful guideline for machining and manufacturing various metallic products.

The future work in this emerging area can be considered with other parameters and different responses such as cutting force, tool life etc. to capture the process in full perspective. The estimation of the reduction of the cost using multi-response optimized EDM process with respect to non-optimized die sinking EDM process can be further investigated. The average cost of energy consumption vs. cost of electrode material (and cost for electrode manufacturing) for the typical product manufactured by EDM process gives a scope for future work.

References

[1] Selvakumar, G., Sarkar, S., Mitra, S. (2013). An experimental analysis of single pass cutting of aluminium 5083 alloy in different corner angles through WEDM, *International Journal of Machining and Machinability of Materials,* Vol. 13, No. 2/3, 262-275, doi: 10.1504/IJMMM.2013.053227.

[2] Kapoor, J., Khamba, J.S., Singh, S. (2012). The effect of machining parameters on surface roughness and material removal rate with cryogenic treated wire in WEDM, *International Journal of Machining and Machinability of Materials*, Vol. 12, No. 1/2, 126-141, doi: 10.1504/IJMMM.2012.048562.

[3] Dvivedi, A., Kumar, P., Singh, I. (2010). Effect of EDM process parameters on surface quality of Al 6063 SiC_p metal matrix composite, *International Journal of Materials and Product Technology,* Vol. 39, No. 3/4, 357-377.

[4] Aligiri, E., Yeo, S.H., Tan, P.C., Zarepour, H. (2010). Benefits of using real-time pulse discriminating system in micro-EDM monitoring and control system, *International Journal of Mechatronics and Manufacturing Systems*, Vol. 3, No. 5/6, 466-481, doi: 10.1504/IJMMS.2010.036070.

[5] Liu, H.S., Tarng, Y.S. (1997). Monitoring of the electrical discharge machining process by abductive networks, *The International Journal of Advanced Manufacturing Technology,* Vol. 13, No. 4, 264-270, doi: 10.1007/BF01179608.

[6] Ayesta, I., Izquierdo, B., Sánchez, J.A., Ramos, J.M., Plaza, S., Pombo, I., Ortega, N., Bravo, H., Fradejas, R., Zamakona, I. (2013). Influence of EDM parameters on slot machining in C1023 aeronautical alloy, In: Lauwers, B., Kruth, J.-P. (eds.), *Procedia CIRP*, *Proceedings of the Seventeenth CIRP Conference on Electro Physical and Chemical Machining (ISEM)*, Vol. 6, Elsevier, 129-134, doi: 10.1016/j.procir.2013.03.059.

[7] Nipanikar, S.R. (2012). Parameter optimization of electro discharge machining of AISI D3 steel material by using Taguchi method, *Journal of Engineering Research and Studies,* Vol. 3, No. 3, 7-10.

[8] Ben Salem, S., Tebni, W., Bayraktar, E. (2011). Prediction of surface roughness by experimental design methodology in electrical discharge machining (EDM), *Journal of Achievements in Materials and Manufacturing Engineering,* Vol. 49, No. 2, 150-157.

[9] Singh, K., Kalra, C.S. (2013). An experimental investigation: machining of OHNS steel by EDM, *Journal of Engineering Computers and Applied Sciences*, Vol. 2, No. 6, 39-42.

[10] Syed, K.H., Palaniyandi, K., (2012). Performance of electrical discharge machining using aluminium powder suspended distilled water, *Turkish Journal of Engineering and Environmental Science*, Vol. 36, 195-207, doi: 10.3906/muh-1202-2.

[11] Kumar, A., Kumar, V., Kumar, J. (2012). Prediction of surface roughness in wire electric discharge machining (WEDM) process based on response surface methodology, *International Journal of Engineering and Technology*, Vol. 2, No. 4, 708-719.

[12] Kohli, A., Wadhwa, A., Virmani, T., Jain, U. (2012). Optimization of material removal rate in electrical discharge machining using fuzzy logic, *World Academy of Science, Engineering and Technology*, Vol. 6, No. 12, 1509-1514.

[13] Mohanty, C.P., Sahu, J., Mahapatra, S.S. (2013). Thermal-structural analysis of electrical discharge machining process, In: Mehta, U. (ed.), *Procedia Engineering, Chemical, Civil and Mechanical Engineering Tracks of 3rd Nirma University International Conference on Engineering*, Vol. 51, 508-513, doi: 10.1016/j.proeng.2013.01.072.

[14] Arikatla, S.P., Krishnaiah, A., Mannan, K.T. (2013). Optimization of electric discharge machining response variables using design of experiments, *International Journal of Mechanical and Production Engineering*, Vol. 2 No. 1, 82-87.

[15] Baseri, H., Aliakbari, E., Alinejad, G. (2012). Investigation of the rotary EDM process of X210Cr12, *International Journal of Machining and Machinability of Materials*, Vol. 11, No. 3, 297-307.

[16] Park, S.H. (1996). *Robust design and analysis for quality engineering*, Chapman and Hall, London.

[17] Montgomery, D.C. (2000). *Design and analysis of experiments,* Fifth edition, John Wiley & Sons, New York.

APEM journal
Advances in Production Engineering & Management
Volume 9 | Number 4 | December 2014 | pp 181–186
http://dx.doi.org/10.14743/apem2014.4.186
ISSN 1854-6250
Journal home: apem-journal.org
Original scientific paper

Effect of welding variables on mechanical properties of low carbon steel welded joint

Talabi, S.I.[a,*], **Owolabi, O.B.**[b], **Adebisi, J.A.**[a], **Yahaya, T.**[a]

[a]Department of Materials and Metallurgical Engineering, University of Ilorin, Ilorin, Nigeria
[b]National Engineering Design Development Institute, Nnewi Anambra State, Nigeria

ABSTRACT

This paper discussed the effect of welding variables on the mechanical properties of welded 10 mm thick low carbon steel plate, welded using the Shielded Metal Arc Welding (SMAW) method. Welding current, arc voltage, welding speed and electrode diameter were the investigated welding parameters. The welded samples were cut and machined to standard configurations for tensile, impact toughness, and hardness tests. The results showed that the selected welding parameters had significant effects on the mechanical properties of the welded samples. Increases in the arc voltage and welding current resulted in increased hardness and decrease in yield strength, tensile strength and impact toughness. Increasing the welding speed from 40-66.67 mm/min caused an increase in the hardness characteristic of the welded samples. Initial decrease in tensile and yield strengths were observed which thereafter increased as the welding speed increased. An electrode diameter of 2.5 mm provided the best combination of mechanical properties when compared to the as received samples. This behaviour was attributed to the fact that increased current and voltage meant increased heat input which could create room for defect formation, thus the observed reduced mechanical properties.

ARTICLE INFO

Keywords:
Welding
Low carbon steel
Welding variables
Mechanical properties

**Corresponding author:*
isaacton@yahoo.com
(Talabi, S.I.)

Article history:
Received 18 September 2014
Revised 3 November 2014
Accepted 10 November 2014

1. Introduction

Steel is an important engineering material. It has found applications in many areas such as vehicle parts, truck bed floors, automobile doors, domestic appliances etc. It is capable of presenting economically a very wide range of mechanical and other properties.

Traditionally mechanical components has been joined through fasteners, rivet joints etc. In other to reduce time for manufacturing, weight reduction and improvement in mechanical properties, welding process is usually adopted. Today, a variety of different welding processes are available, such that welding is extensively used as a fabrication process for joining materials in a wide range of compositions, part shapes and sizes. Welding is an important joining process because of high joint efficiency, simple set up, flexibility and low fabrication costs [1]. Welding is an efficient, dependable and economical process.

Welded joints are finding applications in critical components where failures are catastrophe. Hence, inspection methods and adherence to acceptable standards are increasing. These acceptance standards represent the minimum weld quality which is based upon test of welded specimen containing some discontinuities. Welding involves a wide range of variables such as time, temperature, electrode, pulse frequency, power input and welding speed that influence the

eventual properties of the weld metal [2-9]. Welding of steel is not always easy. There is the need to properly select welding parameters for a given task to provide a good weld quality.

Therefore, the use of the control system in arc welding can eliminate much of the "guess work" often employed by welders to specify welding parameters for a given task [10]. There is therefore need for experimental research to generate data for the design of a welding control system that can give optimized properties.

The effect of welding variables on the mechanical properties of low carbon steel arc welded joints was studied in this research. The experiment was carried out with the object of knowing how these individual variables affect the mechanical properties of the welded steel sample.

2. Materials and methods

The composition of the sample is shown in Table 1. Fig. 1 shows, the welded plate and the geometry of the 10 mm plates butt welded with a weld gap of 3 mm. Specimens of dimensions 60 mm × 40 mm × 10 mm were prepared as suggested by Agarwal [11]. Work piece surfaces and edges were suitably prepared using wire brush prior to the welding processes. The plates were welded together by the SMAW process employing basic coated electrodes. A 7018 low hydrogen electrode rod was used for the welding operation. A high voltage DC generators with rectifiers, capable of supplying current of up to 600 A, air and water cooled electrode holder was used for the welding operation. Pair of prepared metal plates were abutted leaving a gap of about 3 mm in between, while the gap is filled completely, putting into consideration the root, hot pass, fill, cap and bead. The welding was done under controlled and varying welding variables. The welded samples were allowed to cool and tapped with hammer to remove the slag in other to ensure the gap was perfectly filled. The completely filled welded joints were thereafter ground with grinding machine to standard dimension. Four independent process variables, i.e. welding current, welding voltage, welding speed and electrode diameter were selected for study.

Impact tests were conducted using the Avery-Dennison impact-testing machine. Each experiment was repeated at least three times and the average values recorded. Brinell hardness tester under a static load of 3000 kg with a ball indenter of 10 mm diameter was used for the determination of the hardness of the welded joint specimens at a dwell time of 15 s. The diameter of indentation on the specimen was measured with the aid of a calibrated microscope and determined according to ASTM E 10-08 standard and the corresponding hardness obtained. A transverse tensile test specimen was cut from a welded butt joint to determine its transverse tensile strength according to BS EN 895 standard. A Mosanto tensiometer was used to determine the ultimate tensile strength and yield strength of the welded specimen using ISO 6892 standard.

Table 1 Chemical analysis result of as-received low carbon steel (LCS)

Element	C	Si	Mn	P	S	Cr	Nb	Ni	Al	Cu	V
Percentage	0.08	0.35	1.49	0.013	0.002	0.03	0.004	0.17	0.047	0.03	0.001

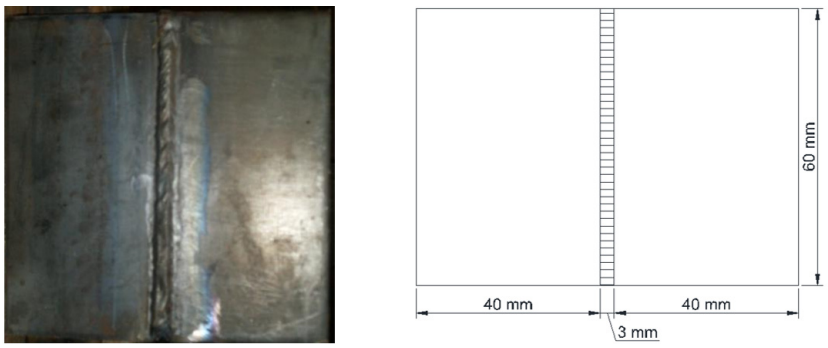

Fig. 1 Welded Plate and the geometry of the 10 mm plates butt welded with a weld gap of 3 mm

3. Result and discussions

3.1 Hardness

Fig. 2 shows the effect of the welding variables on the hardness of welded joint of low carbon steel samples. Fig. 2(a) shows that the hardness of the welded samples changed slightly with changes in voltage values between 20 V and 35 V. The sample welded at 20 V shows a considerable increase in hardness as compared to the unwelded sample which decreased slightly above this voltage value. As seen in Fig. 2(b), increase in the welding current from 95 A to 155 A resulted in increase in hardness. This is similar to the effect of the welding voltage. In Figs. 2(c) and 2(d), the hardness of the samples increased with increasing welding speed while the highest hardness value was obtained with 3.5 mm electrode diameter. Increasing the welding speed from 40 mm/min to 66.67 mm/min caused an increase in the hardness characteristic of the welded samples. This phenomenon can be related to structural changes of weld metal during solidification and chances of formation of defect in the various welding conditions. The weldment increased hardness value may be due to carburization. These increased hardness values indicates that the welded joint will be prone to brittleness than the base metal; hence post-welding heat treated will be required to optimize the mechanical property [12]. The results obtained are similar to the work of other researchers [12-14].

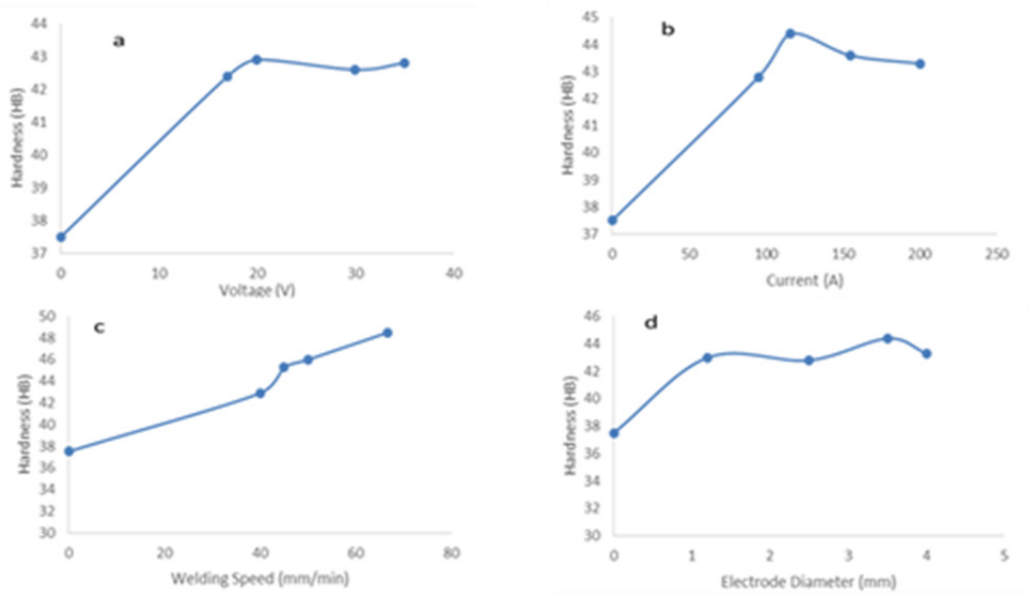

Fig. 2 Effect of welding parameters on the hardness of the welded joint

3.2 Tensile properties

The effect of welding voltage, current, speed and electrode diameter variations with yield strength (MPa) and ultimate tensile strength (UTS, MPa) of the welded joints are shown in Fig. 3 and Fig. 4, respectively. Both figures show that the yield strength and UTS of all the joints decreased with increased voltage. However, increase in welding speed increases both the UTS and yield strength of the welded joints. The current value of 95 A gives the UTS (643.91 MPa) which is closest to the UTS value of unwelded sample (654.91 MPa). Afterward, a significant decrease in UTS value was recorded as the current increased. The decrease in strength may be associated with the presence of void and other defects occurring as a result of increasing current. Excessive grain growth could also lead to the decrease in the tensile properties [15]. This result is also similar to the work of another author [13].

Yield strength decrease of 19.8 %, 34.2 %, 28.4 % and 34.2 % were obtained for the voltage, current, speed, and electrode diameter, respectively, while UTS decreased by 27.8 %, 29.9 %, 27.8 % and 29.8 % for the various welding parameters. It is evident from here that welding current and electrode diameter are important parameters that must be monitored for tensile properties of steel. The welding current must not be too high and electrode diameter of 2.5 mm gave better combination of the tensile properties. It could also be deduced for the figures that the travel speed of 66.67 mm/min has the best tensile properties combination which is close to the as-received samples.

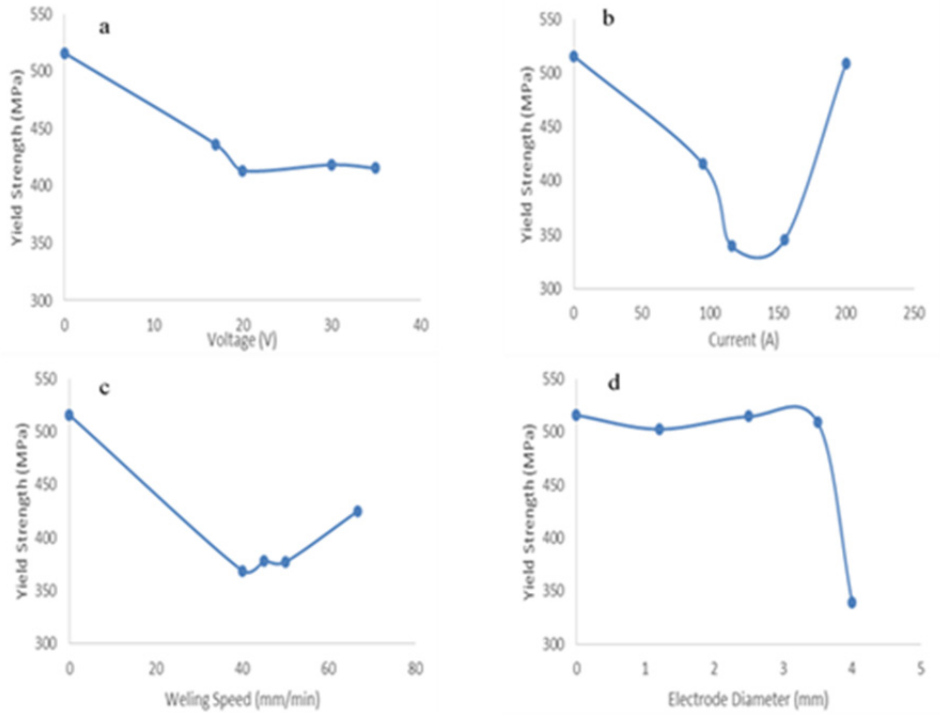

Fig. 3 Effect of welding parameters on the ultimate tensile strength of the welded joint

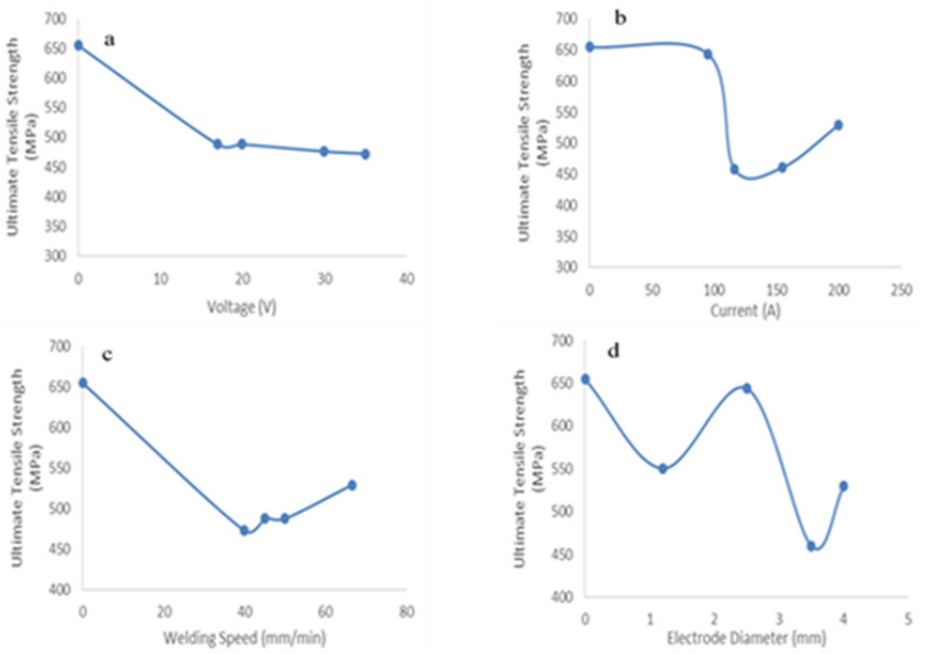

Fig. 4 Effect of welding parameters on the yield strength of the welded joint

3.3 Impact toughness

Fig. 5 shows the effect of welding parameters on the impact toughness of the welded joint made by SMAW. The impact toughness values of all the welded joints are lower than that of the base metal irrespective of the welding parameters. The figure shows similar profile with those of the tensile properties except for welding voltage and electrode diameter. Impact toughness decrease of 12.0 %, 9.1 %, 12.9 %, and 9.5 % were also obtained for welding voltage, current, speed and electrode diameter, respectively, compared with that of the base metal. This shows that welding voltage and speed must be synergistically selected to obtain the best impact toughness value. Electrode diameter of 2.5 mm also gave the best impact value for the welded joints.

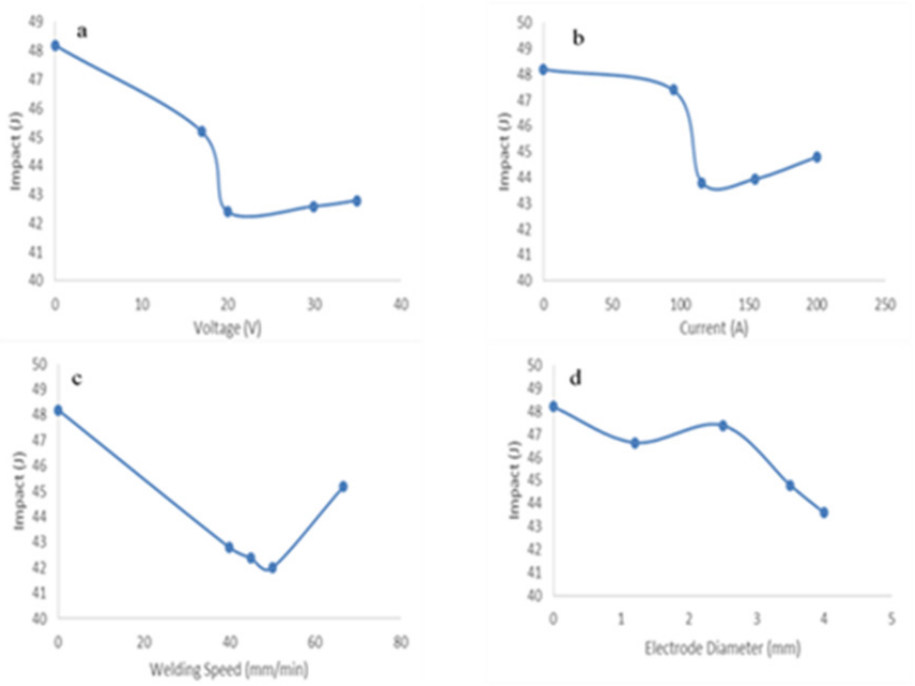

Fig. 5 Effect of the welding parameters on the Impact strength of the weld metal

4. Conclusion

The effect of varied welding parameters was examined and discussed in other to be able to predict the service behaviour (performance) of welded low carbon steel samples. The results have shown that the selected welding parameters have significant effect on the mechanical properties of the welded samples. Increase in the arc voltage and welding current result in increased hardness values and decreased yield strength, tensile strength and impact toughness. This behaviour was attributed to the fact that increased current and voltage means increase in the heat input which can create room for defect formation, thus the observed reduced mechanical properties. The increased hardness may be due to electrode coating which provides alloy addition to the weld deposit. In the future work, the authors plan to report the effect of this welding variable on the microstructure of the steel sample. The structure-properties relationship will also be characterised.

Acknowledgement

The authors wish to acknowledge the contribution of Nigerian Navy Dockyard, Lagos for providing the facility that was used to carry out the experimental work.

References

[1] Armentani, E., Esposito, R., Sepe, R. (2007). The effect of thermal properties and weld efficiency on residual stresses in welding, *Journal of Achievements in Materials and Manufacturing Engineering*, Vol. 20, No. 1-2, 319-322.

[2] Jariyaboon, M., Davenport, A.J., Ambat, R., Connolly, B.J., Williams, S.W., Price, D.A. (2007). The effect of welding parameters on the corrosion behaviour of friction stir welded AA2024-T351, *Corrosion Science*, Vol. 49, No. 2, 877-909, doi: 10.1016/j.corsci.2006.05.038.

[3] Karadeniz, E., Ozsarac, U., Yildiz, C. (2007). The effect of process parameters on penetration in gas metal arc welding processes, *Materials & Design*, Vol. 28, No. 2, 649-656, doi: 10.1016/j.matdes.2005.07.014.

[4] Lothongkum, G., Viyanit, E., Bhandhubanyong, P. (2001). Study on the effects of pulsed TIG welding parameters on delta-ferrite content, shape factor and bead quality in orbital welding of AISI 316L stainless steel plate, *Journal of Materials Processing Technology*, Vol. 110, No. 2, 233-238, doi: 10.1016/S0924-0136(00)00875-X.

[5] Lothongkum, G., Chaumbai, P., Bhandhubanyong, P. (1999). TIG pulse welding of 304L austenitic stainless steel in flat, vertical and overhead positions, *Journal of Materials Processing Technology,* Vol. 89-90, 410-414, doi: 10.1016/S0924-0136(99)00046-1.

[6] Mirzaei, M., Arabi Jeshvaghani, R., Yazdipour, A., Zangeneh-Madar, K. (2013). Study of welding velocity and pulse frequency on microstructure and mechanical properties of pulsed gas metal arc welded high strength low alloy steel, *Materials & Design*, Vol. 51, 709-713, doi: 10.1016/j.matdes.2013.04.077.

[7] Sakthivel, T., Sengar, G.S., Mukhopadhyay, J. (2009). Effect of welding speed on microstructure and mechanical properties of friction-stir-welded aluminum, *The International Journal of Advanced Manufacturing Technology*, Vol. 43, No. 5-6, 468-473, doi: 10.1007/s00170-008-1727-7.

[8] Razal Rose, A., Manisekar, K., Balasubramanian, V. (2012). Influences of welding speed on tensile properties of friction stir welded AZ61A magnesium alloy, *Journal of Materials Engineering and Performance*, Vol. 21, No. 2, 257-265, doi: 10.1007/s11665-011-9889-0.

[9] Afolabi, A.S. (2008). Effect of electric arc welding parameters on corrosion behaviour of austenitic stainless steel in chloride medium, *AU Journal of Technology*, Vol. 11, No. 3, 171-180.

[10] Lee, J.I., Um, K.W. (2000). A prediction of welding process parameters by prediction of back-bead geometry, *Journal of Materials Processing Technology*, Vol. 108, No. 1, 106-113, doi: 10.1016/S0924-0136(00)00736-6.

[11] Agarwal, R.L. (1992). *Welding engineering – a textbook for engineering students*, 4th edition, New Delhi, India, Khanaa Publishers.

[12] Sahin, M. (2005). Joining with friction welding of high-speed steel and medium-carbon steel, *Journal of Materials Processing Technology*, Vol. 168, No. 2, 202-210, doi: 10.1016/j.jmatprotec.2004.11.015.

[13] Das, C.R., Albert, S.K., Bhaduri, A.K., Srinivasan, G., Murty, B.S. (2008). Effect of prior microstructure on microstructure and mechanical properties of modified 9Cr-1Mo steel weld joints, *Materials Science and Engineering: A*, Vol. 477, No. 1-2, 185-192, doi: 10.1016/j.msea.2007.05.017.

[14] Boumerzoug, Z., Raouache, E., Delaunois, F. (2011). Thermal cycle simulation of welding process in low carbon steel, *Materials Science and Engineering: A*, Vol. 530, 191-195, doi: 10.1016/j.msea.2011.09.073.

[15] Gharibshahiyan, E., Raouf, A.H., Parvin, N., Rahimian, M. (2011). The effect of microstructure on hardness and toughness of low carbon welded steel using inert gas welding, *Materials & Design*, Vol. 32, No. 4, 2042-2048, doi: 10.1016/j.matdes.2010.11.056.

APEM journal
Advances in Production Engineering & Management
Volume 9 | Number 4 | December 2014 | pp 187–200
http://dx.doi.org/10.14743/apem2014.4.187
ISSN 1854-6250
Journal home: apem-journal.org
Original scientific paper

A Petri net model for the integration of purchasing, production and packaging using Kanban system

Ullah, H.[a,*]

[a]Mechanical Engineering, Faculty of Engineering, Institut Teknologi Brunei, Jalan Tungku Link, Brunei

ABSTRACT

A new generic deterministically timed Petri net (PN) model was developed for the integration of purchasing, production, and packaging using the Kanban system. Firstly, the individual building blocks of the model were developed which are then combined together to obtain the overall integrated PN model. This model allows the modeling of an integrated production system configuration for determining the optimal Work-In-Process (WIP), lead-time, station's utilization, and rate of production of the system. Each station can have multiple identical servers. The model is solved first by initial marking and then by optimal marking using LINGO software. The machining server circuit with the largest cycle time determines the bottleneck station, as the cycle time of this circuit merely represents the capacity of the corresponding station. Elementary circuits with cycle times greater than the cycle time of the machining server circuit are selected for optimization. These circuits result in constraints. The objective of optimization is to ensure the WIP minimum corresponds to the maximum throughput. The maximum throughput with the minimum WIP is formulated as a linear programming problem. The model can be used for designing, evaluating, and optimizing the layout of an integrated production system. This model could be extended using Fuzzy PN, Coloured PN, or Queuing PN.

ARTICLE INFO

Keywords:
Production
Purchasing
Packaging
Petri net
Kanban

**Corresponding author:*
hamid.ullah@itb.edu.bn
(Ullah, H.)

Article history:
Received 29 June 2014
Revised 13 November 2014
Accepted 18 November 2014

1. Introduction

The birth of modern manufacturing dates to the age of the industrial revolution which started in the middle of the eighteenth century in England and propagated in Europe and in North America. It was due primarily to the invention of the steam engine and the subsequent consequence of the ability to produce products for consumption by mechanization. From a social and economic perspective, it resulted in a significant improvement in wealth and in the standard of living [1]. To respond rapidly to the highly volatile market, the emerging reconfigurable manufacturing systems have brought forward two challenging issues, namely how to build a rapid formal model of an initial manufacturing configuration and how to yield the target model from the existing one along with manufacturing configuration changes [2]. Modeling and performance analysis of manufacturing systems helps decision makers at higher levels to conduct an economic feasibility analysis for diversification and/or modification of the system. Manufacturing systems design is a complex phenomenon, which is concerned with the selection from a wide variety of available system configurations and control strategy alternatives in the light of several criteria (flexibility, quality, productivity, costs etc.), many of which are difficult to quantify [3].

PNs have proved to be effective graphical, mathematical, and simulation tool for discrete event systems. From the design perspective, PNs provide many advantages in modeling, performance evaluation, and qualitative analysis of FMS. However, with the growth in the complexity of modern industrial, and communication systems, PNs were found inadequate to address the problems of uncertainty and imprecision in data. This gave rise to combination of Fuzzy logic, Object-oriented approach, and Queueing theory with PNs and new tools emerged with the names of Fuzzy PNs, Object-oriented PNs, Queueing PNs, and Colored PNs. Object-oriented PNs have been used for performance modeling of a Flexible manufacturing system (FMS) and efficient production control implementation [4]. To minimize makespan for FMSs, deadlock-free scheduling algorithm is used. In the reachability graph of the PN, scheduling is performed as a heuristic search where the search process is guided by a heuristic function [5]. Based on timed PN model of FMS with the goal of minimizing makespan, a hybrid heuristic search approach is presented which combines dynamic search window with best-first algorithm and backtracking search [6]. Generic hybrid PN model combined with the lowest-makespan-cut is used for job shop scheduling problems in mold manufacturing in order to minimize the makespan of the mold part manufacture schedule. The integration of the PN model and the lowest-makespan-cut algorithm can help to improve the production efficiency [7]. A method of modeling parallel processing flows, sharing limited number of resources in FMSs is presented. A new class of PN called parallel process net with resources is introduced for modeling such FMSs. Parallel process net with resources has the capacity to model the more complex resource-sharing among parallel manufacturing processes [8]. Stochastic PNs, together with fuzzy set theory, are used for modeling FMS to represent both stochastic variability and imprecision [9].

1.1 Motivation

The design and operation of modern industrial systems require modeling and analysis in order to select optimal design alternative and operational policy. PNs are graphical and mathematical modeling techniques developed as effective modeling tools for concurrent system operations [10]. Kanban cards pass through a series of events that can easily be included in the PN model. The kanban card in Just-In-Time (JIT) manufacturing has a lot of similarity with a token in a place, so it looks very attractive to model it as such in a PN. Another attractive aspect of PNs is that they can be used both as a simulation model and as an analytic mathematical model. In production system, the WIP is controlled by the number of pallets in the system. In JIT, the number of kanban cards controls the WIP. This is a strong motivation to model and operate production systems with JIT [11]. Furthermore, a PN can model deterministic or stochastic processing times and also presents the assembly sequencing of parts in a clear fashion.

1.2 Flexible manufacturing system

Manufacturing is the economic term for making goods and services available to satisfy human wants. The manufacturing system is an arrangement of physical elements characterized by measurable parameters. A flexible manufacturing concept has emerged due to the progress in manufacturing technology [12]. The entire company is often referred to as the enterprise or the production system [13]. FMS is defined as automated manufacturing system consisting of multifunctional machines interconnected by a material handling system [14]. It is an important tool for increasing the production efficiency and reducing the total production time [15]. Due to constant fluctuations in market demands, FMS is given great importance to improve competitiveness [16].

1.3 Inspection

In order to produce components that meet the design criteria, manufacturing companies have to ensure the components they produce meet the required dimensional and accuracy standards. Inspection is an important aspect of quality control. It ensures what is being manufactured will meet design specifications [13]. It helps to control the quality of products by fixing the sources of defects immediately after they are detected. It is useful for any industry that wants to improve productivity, reduce end-line defects (that impair performance), and save time and efforts of

final inspection. In fact, any quality control system is based on measurements performed on preselected key quality characteristics. Perhaps the most apparent aspect of this link is conformance testing, which should guarantee products functionality. However, any measurement comes with a cost [17].

1.4 Flexible assembly system

Flexible assembly systems (FASs) are "assembly FMSs" [18]. An FAS often consists of a number of robots, material-handling devices, part feeders, computers, storage units, and communication networks etc. Key indicators of flexibility in a FAS are its capability of handling jobs of varying batch volume, varying assembly plans, varying products, and control adaptability etc. FAS has the capability of producing small and medium-sized products and avoids many disadvantages encountered with fixed assembly systems [19]. An FAS maximizes production rate and increases resource utilization by avoiding unnecessary job transfers within the factory. However, to realize the full benefits of FASs, one has to consider their modeling and simulation to investigate problems relating to design, performance optimization, and line control.

1.5 Packaging

In today's stiff competition in every product along with increasing consumer demand, it becomes imperative for companies to explore ways to improve their productivity in terms of maintaining safety, using sustainable packaging materials, implementing flexible and standardized technology, and adopting proven management principles [20]. Packaging can be described as a coordinated system of preparing goods for transport, warehousing, logistics, sale, and end use. Packaging protects, preserves, transports, informs, and sells. In many countries, it is fully integrated into government, business, institutional, industrial, and personal use [21]. Product packaging is as important as one of the market principle including prices, products, places, and promotions. Product packaging adds to the reputation of the manufacturer and also helps to create the brand’s image [22]. Packaging attributes are considered to have an influence on consumer purchasing decisions [23]. Packaging is an important function, enclosing materials and products for distribution and movement [24]. Some of the recent innovations in the field of packaging include development of passive and active packaging, intelligent packaging, and interactive packaging [25].

1.6 Petri nets

A PN is a bipartite directed graph consisting of four primitive elements (i.e., tokens, places, transitions, and arcs) along with rules that govern their operation. Tokens (represented by dots) are conceptual entities used to represent objects moving in an abstract network. Places (represented by circles) show the states of the objects. Places may represent resources such as machines, AGVs, computer code, or parts in a buffer. The existence of a token in a place represents the availability of a resource. Transitions (denoted by bars) represent activities. Places and Transitions together represent conditions and precedence relations in the system’s operation. A transition fires provided there is at least one token in each of the input places of the transition. The places and transitions are connected by directed arcs that represent the sequence of operations [11]. When the specified time is deterministic, the PN is called deterministic timed PN. When a probability distribution to the firing time is assigned, the PN is called a stochastic timed PN. Various colors can be used to distinguish part-types. However, the size of the colored PN model is smaller compared to the PN model due to grouping the places and transitions of PN model into the colored PN model. The use of kanban in PN controls the rate of production according to the demand of a market. Another advantage of kanban in PN is that it provides a better coordination between the upstream and the downstream activities in a manufacturing organization.

This paper presents a new generic deterministic timed PN model for the integration of purchasing, production, and packaging using Kanban system. A production system refers to the total company and includes within it the manufacturing system. The production system includes the manufacturing system, transportation system, inspection system, and assembly system. The

subsystems are integrated together to get an overall integrated PN model. The model can be used for the design and performance evaluation of the system using kanban. The model can be developed using colored PNs. The model can be extended for rejection of parts (if any) during inspection.

The remainder of the paper is structured as follows: section 2 describes Petri net modeling of building blocks. It is followed by development of the proposed Petri net model for integration of purchasing, production, and packaging in section 3. An example/case study is presented in section 4, where the proposed PN model is applied to a ball bearing. Section 5 gives results, discussion, and managerial implications. Conclusion remarks are given in section 6.

2. Petri net modeling of building blocks

As mentioned earlier, first the building blocks of the overall PN model are developed. These building blocks are then combined together to get the PN model for integration of purchasing, production, and packaging. The physical meanings of the symbols used in the PN model are given in Table 1.

Table 1 Symbols and their meanings in the PN model

Symbols	Meaning in the PN model
K_B	Kanban transition for buying/purchasing
K_M	Kanban transition for movement/transportation
K_P	Kanban transition for production/machining
K_I	Kanban transition for inspection
K_A	Kanban transition for assembly
K_{Pa}	Kanban transition for packaging
K_R	Kanban transition for feedback for replenishment
T_B	Processing transition for buying/purchasing
T_T	Processing transition for transportation
T_P	Processing transition for production/machining
T_I	Processing transition for inspection
T_A	Processing transition for assembly
T_{Pa}	Processing transition for packaging
MC	Place for move card
BC	Place for buying/purchasing card
PC	Place for production/machining card
IC	Place for inspection card
AC	Place for assembly card
PaC	Place for packaging card
P_{MA}	Place for material availability
P_B	Place for buying/purchasing associated with buying transition
P_M	Place for movement/transportation associated with move kanban transition
P_p	Place for production associated with production/machining transition
P_T	Place for transportation associated with transportation transition
P_I	Place for inspection associated with inspection transition
P_A	Place for assembly associated with assembly transition
P_{Pa}	Place for packaging associated with packaging transition
P_R	Place for replenishment associated with kanban transition for replenishment
S_B	Place for buying/purchasing server
S_T	Place for movement/transportation server
S_P	Place for production/machining server
S_I	Place for inspection server
S_A	Place for assembly server
S_{Pa}	Place for packaging server
●	Token showing availability of material, part, subassembly, or final assembly

2.1 Petri net model of flexible manufacturing system

Production sequence for a typical part with a feedback for replenishment is shown in Fig. 1. Fig. 2 shows the closed PN model for this production sequence, using kanban.

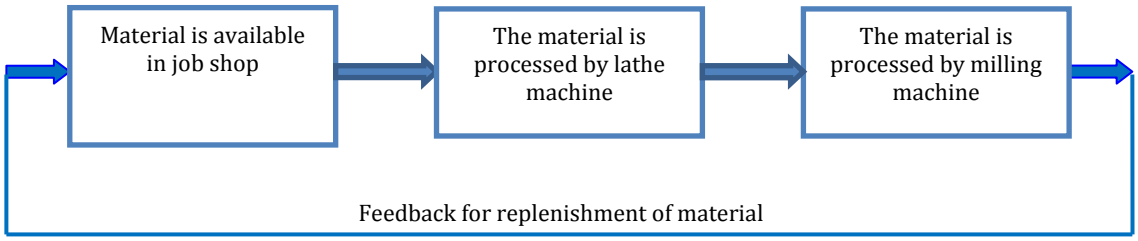

Fig. 1 Production sequence for a typical part

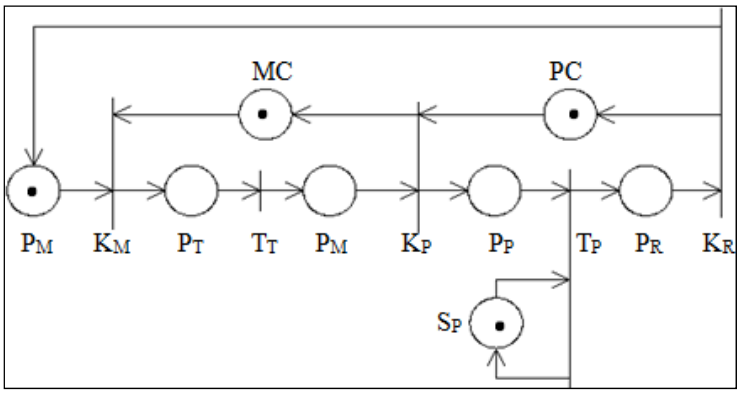

Fig. 2 PN model for Flexible Manufacturing System (FMS)

The availability of a token each in place P_M and place MC enables the kanban transition K_M to fire. After firing of K_M, tokens from places P_M and MC are taken and a token is added to place P_T which an output place for transition K_M. Now, the transition T_T gets enabled and therefore fires. After firing, the token from the input place of transition T_T is withdrawn and a token is added to its output place P_M. Transition K_P gets enabled and fires. Because each of its input places P_M and PC has got a token. After firing, the tokens from places P_M and PC are removed and token is added to each of its output places P_P and MC. The production transition T_P gets enabled because of availability of a token in each of its input places P_P and S_P. After firing of transition T_P, tokens are taken from its input places P_P and S_P and a token is added to each of its output places P_R and S_P. This makes the transition K_R enabled. Firing of K_R removes token from its input places P_R and adds a token to its output place P_M for repetitive manufacturing.

2.2 Petri net model of flexible assembly system

After manufacturing of individual parts, the next stage is their assembly. Fig. 3 shows the PN model for FAS of two parts. The presence of a token each in place P_1 and place P_2 shows the availability of part 1 and part 2 for assembly. The kanban transitions K_{M1} and K_{M2} attach move cards MC_1 and MC_2 to parts P_1 and P_2. After getting authorization for movement, the parts are moved after firing of transportation transitions T_{T1} and T_{T2}. Kanban transitions K_{A1} and K_{A2} detach move cards MC_1 and MC_2 from the two parts and attach assembly cards AC_1 and AC_2 to these parts. Firing of assembly transition T_A assembles the two parts together. The final assembly is shown by place P_R. Firing of transition K_R signals authorization for replenishment of individual parts, in places P_1 and P_2, for cyclic assembly of parts.

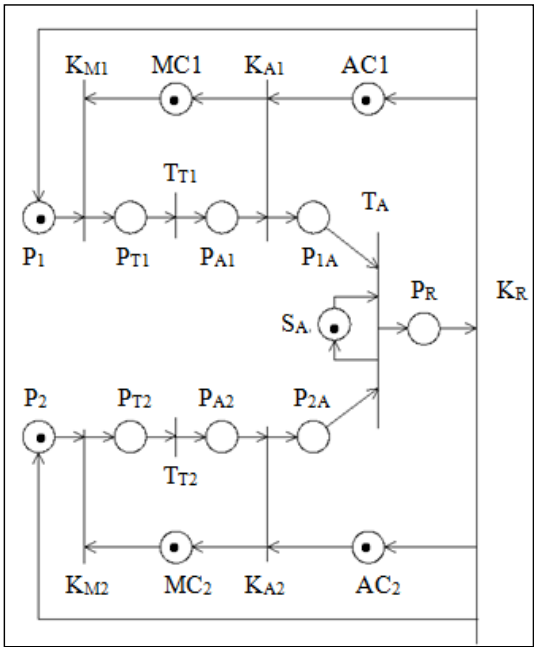

Fig. 3 PN model for Flexible Assembly System (FAS)

2.3 Petri net model of flexible purchasing system

Purchasing is the management of acquisition process. It consists of deciding which suppliers to use, whether to buy locally or centrally, and negotiating contracts. Storage, conversion, and distribution are of strategic importance at the start of the purchasing. It must satisfy the firm's long-term supply needs and support production capabilities of the firm. This task is crucial for every organization, whether it is retailer, service provider, or manufacturer.

Flexible purchasing system (FPS) is defined as a system in which raw material will be purchased by the manufacturing organization and will be supplied by the supplier only when it is required in order to avoid the unnecessary storage of the material in the organization. Purchasing is made flexible by the use of kanban. It will allow supplier to supply material to the manufacturing organization as and when required by the organization. Similarly, the system will allow the organization to demand for the purchase of raw material only when it is required. Thus, the system establishes a good coordination between the supplier and the manufacturing organization. This coordination is established with the help of kanban card called buying card (BC) in our case. Thus, BC will show authorization for buying (purchasing) of raw material.

Fig. 4 shows a closed PN model for FPS of raw material. The token in place P_{MA} shows the availability of the raw material in the market. The availability of the tokens in places P_{MA} and BC enables the kanban transition K_B to fire. Firing of the kanban transition K_B authorizes buying the material from the supplier. Firing of transition K_B takes tokens from its input places P_{MA} and BC and adds a token to its output place P_B. The buying transition T_B gets enabled because a token is available at each of its input places P_B and S_B. Firing of transition T_B withdraws tokens from its input palces and adds a token to its output place P_M. The kanban transition K_M now gets enabled in the presence of a token in each of its input places P_M and MC. Transition K_M shows authorization to detach buying card BC and attach move card MC. After firing of kanban transition K_M, tokens from places P_M and MC are removed and a token is added to each of the places P_T and BC. The presence of a token in place P_T shows that the material is ready to be moved from the supplier to the warehouse. The transportation transition T_T gets enabled and therefore fires. Transition T_T shows the actual transportation time of the material from the supplier to the warehouse. After firing of transition T_T, kanban transition K_R gets enabled and fires to signal authorization for buying material.

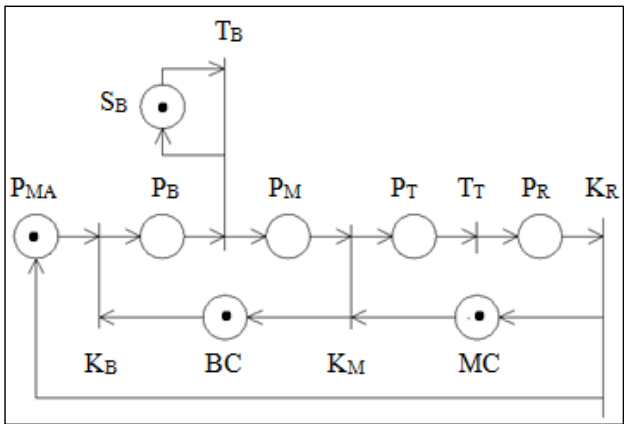

Fig. 4 PN model of Flexible Purchasing System (FPS)

Similarly, building blocks can also be produced, for other functional areas as well, that will be seen in the overall PN model.

3. Development of the proposed Petri net model for integration of purchasing, production, and packaging

Fig. 5 shows a schematic of integration of purchasing, production, and packaging. Initially, raw material is purchased. It is then transported for manufacturing of individual parts. When the parts are manufactured, they are transported for inspection. After meeting the required specifications during inspection, the parts are transported for assembly. Once the final assembly is produced, the product is transported for packaging. After packaging is done, a feedback is given for purchase of raw material for repetitive production. Thus, the key functional areas are working in coordination with each other in the system.

Fig. 6 shows the proposed PN model for the integration of purchasing, production, and packaging. Fig. 7 shows the model with initial marking. Presence of a token in place P_{MA} shows availability of raw material for purchasing. Presence of a token in place BC shows authorization for buying raw material. Kanban transition K_B gets enabled and therefore fires due to availability of a token in each of its input places PM_A and BC. With firing of buying transition T_B raw material is purchased. It is transported to the shop floor, for manufacturing of parts, after firing of transportation transition T_{T1}. Firing of production transitions T_{P1} and T_{P2} manufacture the two parts, which are transported for inspection after firing of transportation transitions T_{T2} and T_{T3}. When inspection transitions T_{I1} and T_{I2} enable and fire, the two parts are inspected and become ready for transportation for assembly. Assembly of the two individual parts, represented by place P_{M6}, takes place when assembly transition T_{A1} gets enabled and fires. Availability of a token in place P_{3T7} shows a third part available for assembly with the subassembly to give a higher subassembly. It is transported for assembly when transportation transition T_{T7} gets fired. When assembly transition T_{A2} gets enabled and fires, this third part is assembled with the subassembly and a higher subassembly represented by place P_{M8} is obtained. A fourth part, represented by a token in place P_{4T9}, is transported for assembly with the higher subassembly after firing of transportation transition T_{T9}. When assembly transition T_{A3} enables and fires, this part is assembled with the higher subassembly to give a final assembly. This final assembly is represented by place P_{M10}. After firing of transportation transition T_{T10}, this final assembly is transported for packaging. When the packaging transition T_{Pa} enables and fires, the packaging operation takes place. With this, the cycle completes, the replenishment transition K_R enables and therefore gets fired. Firing of K_R gives a feedback to the system for buying raw material and replenishment of new individual parts in the input places P_{MA}, P_{3T7} and P_{4T9}. It gives repetitive production.

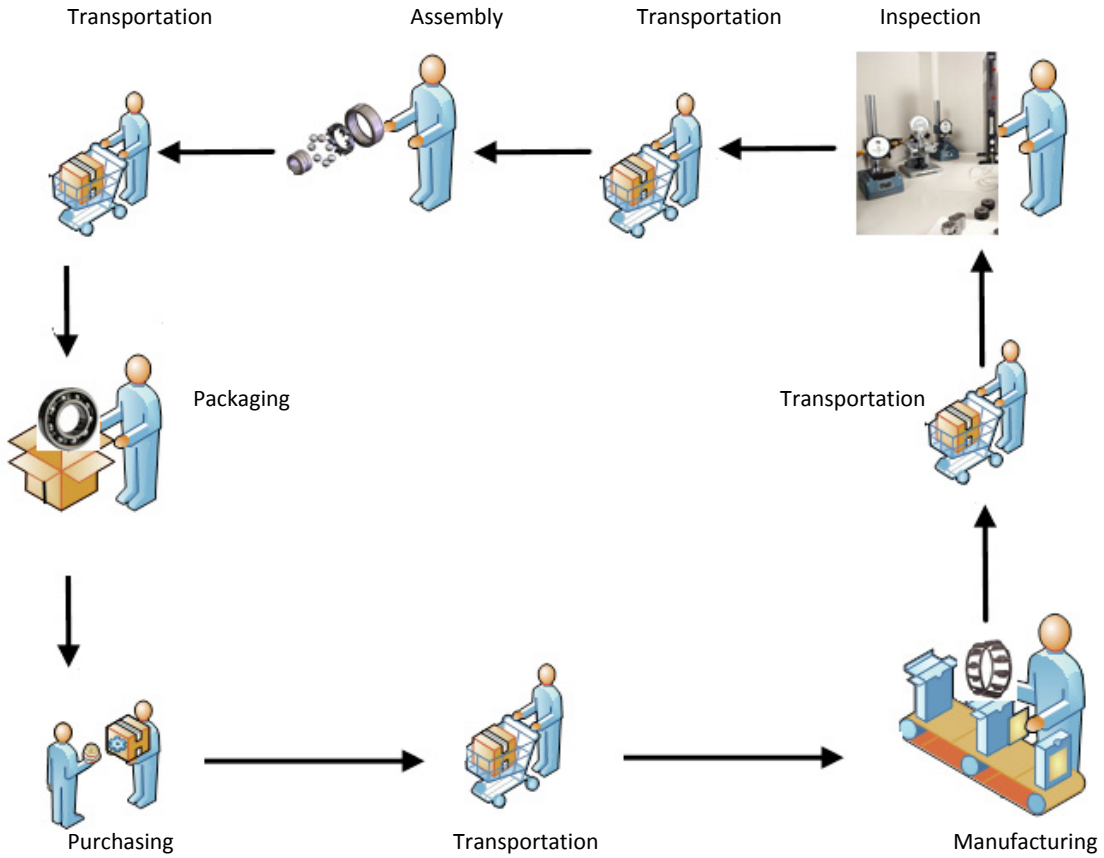

Fig. 5 Schematic of integration of purchasing, production, and packaging

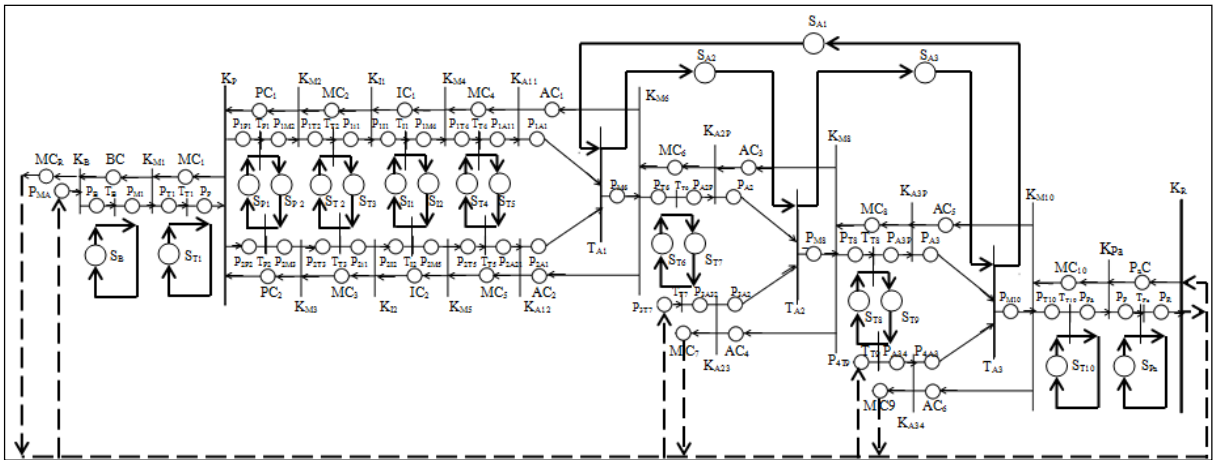

Fig. 6 Petri net model for integration of purchasing, production, and packaging

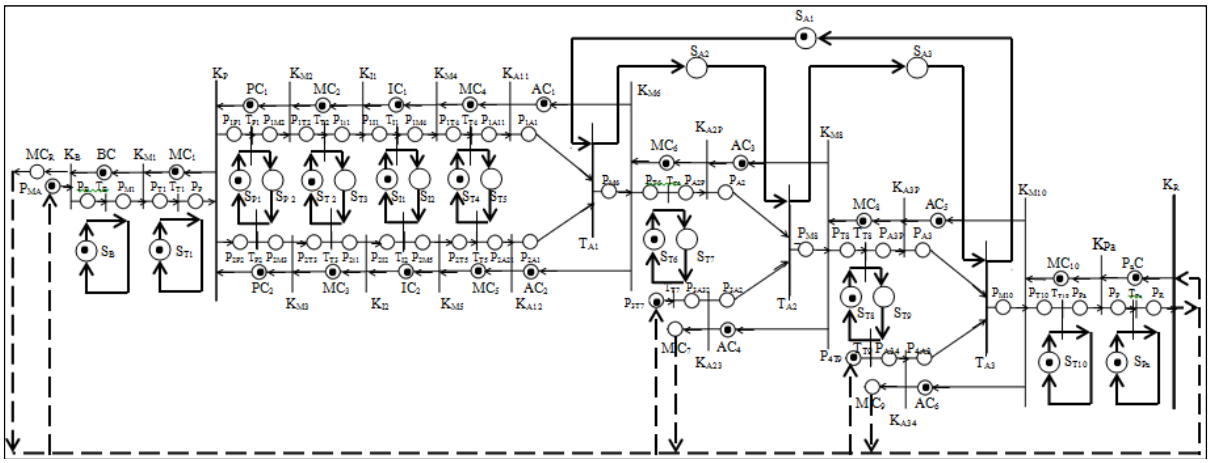

Fig. 7 Petri net model for integration of purchasing, production, and packaging, after initial marking

3.1 Initial marking of the Petri net model

The PN model shown in Fig. 6 and 7 is strongly connected, as there exists a directed path from any node to any other node. The PN is an event graph or decision-free PN because each place has exactly one input transition and one output transition. The initial marking is determined in such a way that the number of tokens in each elementary circuit is at least equal to the maximum arc weight of that elementary circuit. This condition guarantees the liveness of the PN. Physically, this corresponds to a deadlock free FMS. The objective function can be formulated as linear programming problem as follows:

$$\text{MIN} \sum_{i,j} \left(P_i M_j + P_i P_j + P_i T_j + P_i I_j + P_i A_j + P_i Pa_j \right) \tag{1}$$

subject to

$$M(\gamma) \geq w, \qquad \forall \gamma, \tag{2}$$

$$\forall \; P_i P_j, P_i M_j, P_i I_j, P_i A_j, P_i Pa_j \in IN_0 \tag{3}$$

$$\forall \, BC_i, MC_i, PC_i, IC_i, P_a C_i, S_{Bi}, S_{Pi}, S_{Ti}, S_{Ii}, S_{Ai}, S_{Pai} \in IN_0 \tag{4}$$

where $M(\gamma)$ is the sum of tokens in the places of circuit γ. Place names represent the number of tokens in the places which belong to that circuit. Some simple rule to do this can be given: all the parts/kanban circuits should contain one token. The rule of thumb is to put a token in a kanban place instead of a part place because it does not increase WIP.

The total transition time $\tau(\gamma)$ in each elementary circuit γ is determined as the sum of the transition firing times in that elementary circuit:

$$\tau(\gamma) = \sum_{i=1}^{m} \tau(t_i) \tag{5}$$

The total number of tokens $M(\gamma)$ in each elementary circuit γ is obtained as the sum of the number of tokens in that circuit:

$$M(\gamma) = \sum_{j=1}^{n} \left(\frac{M_0(p_j)}{w} \right) \tag{6}$$

where M_0 stands for initial marking. The cycle time $C(\gamma)$ of each elementary circuit is the ratio between the total transition time of the circuit $\tau(\gamma)$ and the total number of tokens $M(\gamma)$ in that circuit:

$$C(\gamma) = \frac{\tau(\gamma)}{M(\gamma)} \tag{7}$$

3.2 Optimal marking of the Petri net model

Let $C(\gamma_c)$ be the largest cycle time of an elementary circuit. This elementary circuit will be called a critical circuit. The cycle time in steady-state is given by the maximum cycle time taken over all elementary circuits. Increasing the number of tokens in each elementary circuit reduces the cycle time of the elementary circuits. The machining server circuit (also called machining sequencing circuit) with the largest cycle time will limit the maximum throughput. In other words, this station will be the bottleneck station. It is possible to increase the number of tokens in non-server circuits in such a way that the machining server circuit becomes the critical circuit. Hence, the objective is keeping WIP minimum corresponding to the maximum throughput. The maximum throughput with minimum WIP is formulated as a linear programming problem:

$$\text{MIN} \sum_{i,j} \left(P_i M_j + P_i P_j + P_i T_j + P_i I_j + P_i A_j + P_i P a_j \right) \tag{8}$$

where i = 1, 2, 3,... shows the number of part in the model, whereas j = 1, 2, 3,... shows the number of the activity/operation (manufacturing, movement, and assembly etc.). The place names stand for the number of tokens in that place subject to:

$$C(\gamma) \leq C(\gamma_c) \tag{9}$$

where

$$\gamma \in \{\gamma : C(\gamma) \geq C(\gamma_c)\} \tag{10}$$

Elementary circuits with cycle times greater than the cycle time of the machining server circuit are selected for optimization, since the cycle time of the machining server circuit merely represents the capacity of the corresponding station.

3.3 Calculation of station utilization and lead time for the Petri net model

The utilization U_j of each station j can be calculated as the ratio of the cycle time of the server circuit j and the cycle time of the critical circuit.

$$U_j = \frac{C(\gamma_{sj})}{C(\gamma_c)} \tag{11}$$

where, γ_{sj} represents the server circuit for station j. The lead time LT can be determined by using Little's law**.** The WIP and critical cycle time are known so the lead time can be calculated:

$$LT_i = C(\gamma_c) \sum_{i,j} \left(P_i M_j + P_i P_j + P_i T_j + P_i I_j + P_i A_j + P_i Pa_j \right) \tag{12}$$

The number of kanban cards in kanban places is determined by the following formula:

$$N_{kc} = \sum (P_i + KC_i) \tag{13}$$

where N_{kc} shows the number of kanban cards. The part places P_i stand for the number of kanban cards attached with parts, subassemblies, or final assembly. The kanban places KC_i show the number of kanban cards in the kanban places.

4. Case study

The proposed PN model is applied to a ball bearing. The designation of the ball bearing is SKF TAM 6208. The bearing consists of four parts: outer race, inner race, balls, and cage. The two races are almost made in the same way, i.e. by CNC lath machines. First, the inner race is inserted inside the outer race, with some eccentricity. Then balls are inserted between the two races. At the final stage of the assembly, the cages are riveted on both sides to equally distribute the balls around the inner race, and lock the balls between the races. The assembly sequence of the ball bearing is shown in Fig. 8.

The INA (Integrated network analyzer) software by Starke is a tool package supporting the analysis of Place/Transition Nets (PNs) and Colored PNs (*http://www2.informatik.hu-berlin.de*) and is used to determine the elementary circuits in the PN model. The elementary circuits given by INA, their cycle times, and initial marking are shown in Table 2.

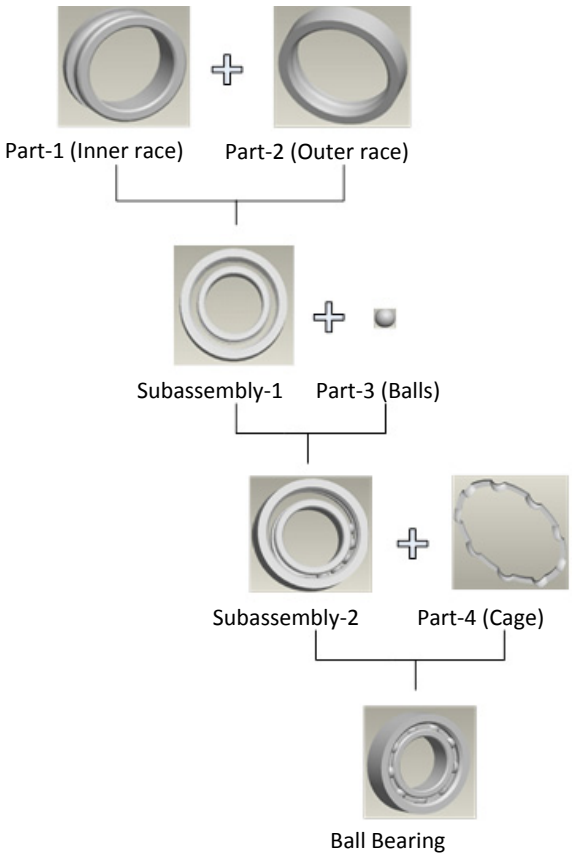

Fig. 8 Assembly sequence of a ball bearing

Table 2 Elementary circuits and their corresponding cycle times for PN model shown in Fig. 7 (a split window is shown)

TM	0	0	0	2	0	0	1	0	0	20	0	0	20			
TRAN	KR	KB	KB	TB	KM1	KM1	TT1	KP	KP	TP1	KM2	KP	TP2			
TOK	0	1	1	0	0	1	0	0	1	0	0	1	0			
PLACE	MCR	PMA	BC	PB	PM1	MC1	PT1	PP	PC1	P1P1	P1M2	PC2	P2P2			
No.	1	2	3	4	5	6	7	8	9	10	11	12	13	M(g)	t(g)	C(g)
1	0	1	0	1	1	0	1	1	0	1	0	0	0	1	61	61
2	0	1	0	1	1	0	1	1	0	1	0	0	0	1	60	60
3	0	1	0	1	1	0	1	1	0	1	0	0	0	1	60	60
4	0	1	0	1	1	0	1	1	0	1	0	0	0	1	59	59
5	0	1	0	1	1	0	1	1	0	1	0	0	0	1	59	59
6	0	1	0	1	1	0	1	1	0	1	0	0	0	1	59	59
7	0	1	0	1	1	0	1	1	0	1	0	0	0	1	58	58
8	0	1	0	1	1	0	1	1	0	1	0	0	0	1	58	58
9	0	1	0	1	1	0	1	1	0	1	0	0	0	1	57	57
10	0	1	0	1	1	0	1	1	0	1	0	0	0	1	55	55
11	0	1	0	1	1	0	1	1	0	1	0	0	0	1	54	54
12	0	1	0	1	1	0	1	1	0	1	0	0	0	1	53	53
13	0	1	0	1	1	0	1	1	0	1	0	0	0	1	52	52
14	0	1	0	1	1	0	1	1	0	1	1	0	0	1	43	43
15	0	1	0	1	1	0	1	1	0	1	1	0	0	1	42	42
16	0	1	0	1	1	0	1	1	0	1	1	0	0	1	42	42
17	0	1	0	1	1	0	1	1	0	1	1	0	0	1	42	42

After initial marking, the next step is to optimize the PN for keeping WIP minimum corresponding to the maximum throughput. For this purpose, the machining server circuit is made the bottleneck station because the cycle time of this circuit merely represents the capacity of the corresponding station. To do this, all those part circuits are considered of which cycle time is greater than the cycle time of the machining server circuit, after the initial marking stage. These part circuits result in constraints. Total twenty seven (27) elementary circuits appear as constraints. The cycle time of these circuits is made equal to or lower than the cycle time of the machining server circuit by putting more tokens in these circuits. LINGO is used for optimization of the PN model. The objective function for the system optimization based on equation (8) is as follows.

MIN: PMA + PB + PM1 + PT1 + PP + P1P1 + P1M2 + P2P2 + P2M3 + P1T2 + P1i1 + P2T3 + P2i1 + P1I1 + P1M4 + P2I2 + P2M5 + P1T4 + P1A11 + P2T5 + P2A21 + P1A1 + P2A1 + PM6 + PT6 + PA2P + P3T7 + P3A32 + PA2 + P3A2 + PM8 + PT8 + PA3P + P4T9 + PA34 + PA3 + P4A3 + PM10 + PT10 + PPa + PP + PR

Each place name represents the number of tokens in that place.

5. Results, discussion, and managerial implications

Total twenty seven (27) elementary circuits appear as constraints. The tokens to be added to the part circuits can be determined by dividing the cycle time of the part circuit with the cycle time of the critical circuit. The number of tokens to be added to the part circuits should be greater than or equal to 1.525, 1.5, 1.475, 1.45, 1.425, 1.375, 1.35, 1.325, 1.3, 1.075, 1.05, and 1.025. After optimization, the performance measures are calculated for the system as shown in Tables 3 and 4. Table 3 shows the total WIP in the system of four (4), the cycle time and lead time of 40 time unit, the throughput (or rate of production) of 0.025 product per unit time, and the total cycle time of the system of 65 time unit. Table 4 shows the optimal values of machine utilization for each station, calculated by dividing the cycle time of a corresponding station by the critical cycle time of the system. This table shows 100 % utilization for the machining station while that of all other stations is lower than 100 %, the minimum being for purchasing station. It is because the machining server circuit with the largest cycle time determines the bottleneck station. The production is bounded by the utilization of this bottleneck station. Table 5 shows the number of kanban cards in the system as follow: buying card is 1, productions cards are 2, move cards are

13, inspection cards are 2, assembly cards are 6, and packaging card is 1. Total number of kanban cards is twenty five (25).

Using the model, there can be a better coordination among all the functional areas involved in the system. The model can also provide managers a better coordination both with the suppliers and the end users. It can help them in coordination and cooperation of the enterprise's overall operation. This coordination will lead to JIT activities in the system. It will result in minimum WIP, less lead time, more throughput, and better product quality. Managers can choose among desired performance measures in order to achieve production management and control. The determination of the total WIP, total number of stations in the system, and the number of servers at each station will help in factory floor management. It will result in greater production efficiency along with ease of supervision.

Table 3 Performance measures for the system

WIP	Cycle time (time unit)	Lead time (time unit)	Throughput (product/time unit)	Total cycle time of system (time unit)
4	40	40	0.025	65

Table 4 Stations utilization in the system

Station's name	Station's utilization
Purchasing station	(2/40) × 100 = 5 %
Machining station	(40/40) × 100 = 100 %
Inspection station	(4/40) × 100 = 10 %
Assembly station	(6/40) × 100 = 15 %
Packaging station	(3/40) × 100 = 7.5 %

Table 5 Number of kanban cards in the system given by Lingo

Purchasing cards	Production cards	Move cards	Inspection cards	Assembly cards	Packaging cards
1	2	13	2	6	1
Total kanban cards					**25**

6. Conclusion

A generic deterministic PN model for the integration of purchasing, production, and packaging is developed in a pull environment using kanban. The performance evaluation of the PN model is based on solution of a linear programming problem. The optimization of the PN model is influenced by the utilization of the bottleneck station. The PN model gives minimum WIP for maximum production rate. Minimum WIP leads to less lead time. Also, the PN model provides a better coordination among the supplier, production manager, quality assurance unit, assembly manager, and packaging, and the end user. Because of this better coordination, JIT activities will take place. In future work, the model can be developed using Fuzzy PN, Colored PN, or Queuing PN.

Acknowledgement

The author would like to express his sincere thanks to the anonymous reviewers for their insightful comments that helped improving quality of the paper.

References

[1] Bassim, M.N. (2014). 8.11 – Economic implications of impact of manufacturing on environment and health, In: Hashmi, S. (ed.), *Comprehensive Materials Processing*, Vol. 8, Elsevier, 199-210, doi: 10.1016/B978-0-08-096532-1.00817-7.

[2] Li, J., Dai, X., Meng, Z., Dou, J., Guan, X. (2009). Rapid design and reconfiguration of Petri net models for reconfigurable manufacturing cells with improved net rewriting systems and activity diagrams, *Computers & Industrial Engineering*, Vol. 57, No. 4, 1431-1451, doi: 10.1016/j.cie.2009.07.013.

[3] Zhang, H., Gu, M. (2009). Modeling job shop scheduling with batches and setup times by timed Petri nets, *Mathematical and Computer Modelling*, Vol. 49, No. 1-2, 286-294, doi: 10.1016/j.mcm.2008.03.010.
[4] Başak, Ö., Albayrak, Y.E. (2014). Petri net based decision system modeling in real-time scheduling and control of flexible automotive manufacturing systems, *Computers & Industrial Engineering*, In Press, Available online 13 October 2014, doi: 10.1016/j.cie.2014.09.024.
[5] Lei, H., Xing, K., Han, L., Xiong, F., Ge, Z. (2014). Deadlock-free scheduling for flexible manufacturing systems using Petri nets and heuristic search, *Computers & Industrial Engineering*, Vol. 72, 297-305, doi: 10.1016/j.cie.2014.04.002.
[6] Wang, Q., Wang, Z. (2012). Hybrid heuristic search based on Petri net for FMS scheduling, In: Xiong, J. (ed.), *Energy Procedia, International Conference on Future Electrical Power and Energy Systems,* Vol. 17, Part A, Elsevier, 506-512, doi: 10.1016/j.egypro.2012.02.128.
[7] Wongwiwat, A., Bohez, E.L.J., Pisuchpen, R. (2013). Production scheduling for injection molding manufacture using Petri net model, *Assembly Automation*, Vol. 33, No. 3, 282-293, doi: 10.1108/AA-12-2013-063.
[8] Ahmad, F., Huang, H., Wang, X.-L. (2010). Petri net modeling and deadlock analysis of parallel manufacturing processes with shared-resources, *The Journal of Systems and Software*, Vol. 83, No. 4, 675-688, doi: 10.1016/j.jss.2009.11.705.
[9] Tüysüz, F., Kahraman, C. (2010). Modeling a flexible manufacturing cell using stochastic Petri nets with fuzzy parameters, *Expert Systems with Applications*, Vol. 37, No. 5, 3910-3920, doi: 10.1016/j.eswa.2009.11.026.
[10] Murata, T. (1989). Petri nets: properties, analysis and applications, In: *Proceedings of the IEEE*, Vol. 77, No. 4, 541-580.
[11] Bohez, E.L.J. (2004). A new time Petri net model for design and performance analysis of a dual kanban FMS, *International Journal of Production Research*, Vol. 42, No. 4, 719-740, dio: 10.1080/00207540310001602900.
[12] Qiao, G., Lu, R.F., Riddick, F. (2003). Flexible modeling and simulation for mass customization manufacturing, In: *Proceedings of the 2003 IIE Annual Conference*, Portland, USA.
[13] Black, J.T., Ronald, A.K. (2011). *DeGarmo's materials and processes in manufacturing*, 11th edition, Wiley.
[14] Jain, A., Jain, P.K., Singh, I.P. (2006). Performance modeling of FMS with flexible process plans – a Petri net approach, *International Journal of Simulation Modeling*, Vol. 5, No. 3, 101-113, doi: 10.2507/IJSIMM05(3)2.064.
[15] Tashnizi, E.S., Farahani, S.N., Nahrekhalaji, A.R.F. (2008). Production process optimization in flexible manufacturing system using Petri nets, In: *Proceedings of the World Congress on Engineering and Computer Science*, San Francisco, USA, 694-698,
[16] Mujica, M., Piera, M.A., Narciso, M. (2010). Revisiting state space exploration of timed coloured Petri net models to optimize manufacturing system's performance, *Simulation Modeling Practice and Theory*, Vol. 18, No. 9, 1225-1241, doi: 10.1016/j.simpat.2010.04.010.
[17] Moroni, G., Petrò, S. (2013). Inspection strategies and multiple geometric tolerances, In: Jiang, X.J., Mathieu, L., Weckenmann, A., (eds.), *Procedia CIRP*, *12th CIRP Conference on Computer Aided Tolerancing*, Huddersfield, UK, Vol. 10, Elsevier, 54-60, doi: 10.1016/j.procir.2013.08.012.
[18] Andreasen, M.M., Ahm, T. (1988). *Flexible assembly system,* IFS Publications, Springer-Verlag, UK.
[19] Zha, X.F., Lim, S.Y.E., Lu, W.F. (2003). A knowledge intensive multi-agent system for cooperative/collaborative assembly modeling and process planning, *Journal of Integrated Design and Process Science*, Vol. 7, No. 1, 99-122.
[20] Mahalik, N.P., Nambiar, A.N. (2010). Trends in food packaging and manufacturing systems and technology, *Trends in Food Science & Technology*, Vol. 21, No. 3, 117-128, doi: 10.1016/j.tifs.2009.12.006.
[21] Soroka, W. (2002). *Fundamentals of packaging technology*, 3rd edition, Institute of Packaging Professionals, Naperville, USA.
[22] Auttarapong, D. (2012). Package design expert system based on relation between packaging and perception of customer, In: Kaewkhao, J., Limsuwan, P., Yupapin, P., Janjai, S. (eds.), *Procedia Engineering*, Vol. 32, Elsevier, 307-314, doi: 10.1016/j.proeng.2012.01.1272.
[23] Koutsimanis, G., Getter, K., Behe, B., Harte, J., Almenar, E. (2012). Influences of packaging attributes on consumer purchase decisions for fresh produce, In: Yeomans, M. (ed.), *Appetite*, *The 36th Annual Meeting of the British Feeding and Drinking Group*, Vol. 59, No. 2, Elsevier, 270-280, doi: 10.1016/j.appet.2012.05.012.
[24] Parvini, M. (2011). 9 – Packaging and material handling, In: Farahani, R., Rezapour, S., Kardar, L. (eds.), *Logistics operations and Management*, Elsevier, 155-180, doi: 10.1016/B978-0-12-385202-1.00009-8.
[25] Singh, R.P., Heldman, D.R. (2014). Chapter 15 – Packaging concepts, In: *Introduction to food engineering*, 5th edition, Academic Press, 767-791, doi: 10.1016/B978-0-12-398530-9.00015-2.

Calendar of events

- The IEEE International Conference on Industrial Engineering and Engineering Management (IEEM 2014), Selangor/KL, Malaysia, December 9-12, 2014.
- International Conference on Artificial Intelligence and Manufacturing Engineering (ICAIME 2014), Dubai, United Arab Emirates, December 25-26, 2014.
- International Conference on Trends in Mechanical Engineering (MEC 2014), Chennai, India, December 27-28, 2014.
- 2nd International Conference on Recent Trends in Engineering and Technology (ICRTET 2015), Cochin, Kerala, India, January 10-11, 2015.
- 4th International Conference on Operations Research and Enterprise Systems (ICORES 2015), Lisbon, Portugal, January 10-12, 2015.
- 3rd International Conference on Laser and Plasma Application in Materials Science (LAPAMS 2015), Kolkata, India, January 15-17, 2015.
- International Conference on Advances in Mechanical Engineering (AME 2015), Dubai, United Arab Emirates, January 23-24, 2015.
- XIII International Conference on Industrial Engineering and Management Systems (ICIEMS 2015), Paris, France, January 23-24, 2015.
- 39th International Conference and Expo on Advanced Ceramics and Composites, Daytona Beach, Florida, USA, January 25-30, 2015.
- XIII International Conference on Industrial Engineering and Operations Management (ICI-EOM 2015), Istanbul, Turkey, January 26-27, 2015.
- The 2nd International Materials, Industrial, and Manufacturing Engineering Conference (MIMEC2015), Bali, Indonesia, February 4-6, 2015.
- International Conference on Design, Manufacturing and Mechatronics, Pune, Maharashtra, India, February 11-13, 2015.
- 6th International Conference on Automation, Robotics and Applications (ICARA 2015), Queenstown, New Zealand, February 17-19, 2015.
- XIII International Conference on Sustainable Intelligent Manufacturing (ICSIM 2015), Paris, France, February 23-24, 2015.
- International Symposium Additive Manufacturing, Dresden, Germany, February 25-26, 2015.
- International Conference on Industrial Engineering and Operations Management (IEOM 2015), Dubai, United Arab Emirates, March 3-5, 2015.
- 6th International Conference on Mechanical, Industrial, and Manufacturing Technologies (MIMT 2015), Melaka, Malaysia, March 6-7, 2015.
- IEEE International Conference on Industrial Technology, Seville, Spain, March 17-19, 2015.
- 4th International Conference on Manufacturing and Industrial Engineering (ICMIE 2015), Singapore, March 21-23, 2015.
- The Seventh International Conference on Adaptive and Self-Adaptive Systems and Applications (ADAPTIVE 2015), Nice, France, March 22-27, 2015.
- 20th International Conference on Wear of Materials, Toronto, Canada, April 12-16, 2015.
- The 4th International Conference on Manufacturing Engineering and Process (ICMEP 2015), Paris, France, April 13-14, 2015.

- 2nd International Conference on New Technologies (NT 2015), Mostar, Bosnia and Herzegovina, April 24-25, 2015.
- IEEE International Conference on Technologies for Practical Robot Applications, Woburn, Massachusetts, USA, May 11-12, 2015.
- IFAC Symposium on Information Control in Manufacturing (INCOM 2015), Ottawa, Canada, May 11-13, 2015.
- 14th International Conference on Tribology (SERBIATRIB 2015), Belgrade, Serbia, May 13-15, 2015.
- International Conference on Advances in Mechanical Engineering (ICAME 2015), Istanbul, Turkey, May 13-15, 2015.
- IEEE International Conference on Robotics and Automation, Seattle, Washington, USA, May 25-30, 2015.
- 2nd International Conference on Industrial Engineering, Management Science and Applications (ICIMSA 2015), Tokyo, Japan, May 26-28, 2015.
- 6th International Conference on Modeling, Simulation and Applied Optimization, Istanbul, Turkey, May 27-29, 2015.
- 10th International Conference on Additive Manufacturing & 3D Printing, Nottingham, UK, July 7-9, 2015.
- 27th European Conference on Operational Research (EURO 2015), Glasgow, UK, July 12-15, 2015.
- The 5th International Conference on Simulation and Modeling Methodologies, Technologies and Applications (SIMULTECH 2015), Colmar, France, July 21-23, 2015.
- XXIV International Materials Research Congress (IMRC 2015), Cancon, Mexico, August 16-20, 2015.
- IEEE 20th Conference on Emerging Technologies & Factory Automation, Luxembourg, Luxembourg, September 8-11, 2015.
- IEEE/RSJ International Conference on Intelligent Robots and Systems (IROS 2015), Hamburg, Germany, September 28 – October 2, 2015.

Notes for contributors

General

Articles submitted to the *APEM journal* should be original and unpublished contributions and should not be under consideration for any other publication at the same time. Extended versions of articles presented at conferences may also be submitted for possible publication. Manuscript should be written in English. Responsibility for the contents of the paper rests upon the authors and not upon the editors or the publisher. Authors of submitted papers automatically accept a copyright transfer to *Production Engineering Institute*, *University of Maribor*.

Submission of papers

A submission must include the corresponding author's complete name, affiliation, address, phone and fax numbers, and e-mail address. All papers for consideration by *Advances in Production Engineering & Management* should be submitted by e-mail to the journal Editor-in-Chief:

Miran Brezocnik, Editor-in-Chief
UNIVERSITY OF MARIBOR
Faculty of Mechanical Engineering
Production Engineering Institute
Smetanova ulica 17, SI – 2000 Maribor
Slovenia, European Union
E-mail: editor@apem-journal.org

Manuscript preparation

Manuscript should be prepared in *Microsoft Word 2007* (or higher version) word processor. *Word .docx* format is required. Papers on A4 format, single-spaced, typed in one column, using body text font size of 11 pt, should have between 8 and 12 pages, including abstract, keywords, body text, figures, tables, acknowledgements (if any), references, and appendices (if any). The title of the paper, authors' names, affiliations and headings of the body text should be in *Calibri* font. Body text, figures and tables captions have to be written in *Cambria* font. Mathematical equations and expressions must be set in *Microsoft Word Equation Editor* and written in *Cambria Math* font. For detail instructions on manuscript preparation please see instruction for authors in the *APEM journal* homepage *apem-journal.org*.

The review process

Every manuscript submitted for possible publication in the *APEM journal* is first briefly reviewed by the editor for general suitability for the journal. Notification of successful submission is sent. After initial screening the manuscript is passed on to at least two referees. A double-blind peer review process ensures the content's validity and relevance. Optionally, authors are invited to suggest up to three well-respected experts in the field discussed in the article who might act as reviewers. The review process can take up to eight weeks. Based on the comments of the referees, the editor will take a decision about the paper. The following decisions can be made: accepting the paper, reconsidering the paper after changes, or rejecting the paper. Accepted papers may not be offered elsewhere for publication. The editor may, in some circumstances, vary this process at his discretion.

Proofs

Proofs will be sent to the corresponding author and should be returned within 3 days of receipt. Corrections should be restricted to typesetting errors and minor changes.

Offprints

An e-offprint, i.e., a PDF version of the published article, will be sent by e-mail to the corresponding author. Additionally, one complete copy of the journal will be sent free of charge to the corresponding author of the published article.

APEM journal

Advances in Production Engineering & Management

Production Engineering Institute (PEI)
University of Maribor
APEM homepage: apem-journal.org

Volume 9 | Number 4 | December 2014 | pp 155-204

Contents

Scope and topics 158

Laser cladding of Ti-6Al-4V alloy with vanadium carbide particles 159
El-Labban, H.F.; Mahmoud, E.R.I.; Al-Wadai, H.

Parametric study of die sinking EDM process on AISI H13 tool steel using statistical techniques 168
Bose, G.K.; Mahapatra, K.K.

Effect of welding variables on mechanical properties of low carbon steel welded joint 181
Talabi, S.I.; Owolabi, O.B.; Adebisi, J.A.; Yahaya, T.

A Petri net model for the integration of purchasing, production and packaging using Kanban system 187
Ullah, H.

Calendar of events 201

Notes for contributors 203

ISSN 1854-6250

apem-journal.org